DOCK8 regulates lymphocyte shape integrity for skin antiviral immunity

Qian Zhang,[1] Christopher G. Dove,[1]* Jyh Liang Hor,[5,6]*
Heardley M. Murdock,[1] Dara M. Strauss-Albee,[1] Jordan A. Garcia,[1]
Judith N. Mandl,[2] Rachael A. Grodick,[1] Huie Jing,[1]
Devon B. Chandler-Brown,[1] Timothy E. Lenardo,[1] Greg Crawford,[7]
Helen F. Matthews,[3] Alexandra F. Freeman,[4] Richard J. Cornall,[7]
Ronald N. Germain,[2] Scott N. Mueller,[5,6] and Helen C. Su[1]

[1]Laboratory of Host Defenses, [2]Laboratory of Systems Biology, [3]Laboratory of Immunology, and [4]Laboratory of Clinical Infectious Diseases, National Institute of Allergy and Infectious Diseases, National Institutes of Health, Bethesda, MD 20892
[5]Department of Microbiology and Immunology, Peter Doherty Institute for Infection and Immunity, and [6]The ARC Centre of Excellence in Advanced Molecular Imaging, University of Melbourne, Parkville, Victoria 3010, Australia
[7]MRC Human Immunology Unit, Nuffield Department of Medicine, Oxford University, Oxford OX3 7BN, England, UK

DOCK8 mutations result in an inherited combined immunodeficiency characterized by increased susceptibility to skin and other infections. We show that when DOCK8-deficient T and NK cells migrate through confined spaces, they develop cell shape and nuclear deformation abnormalities that do not impair chemotaxis but contribute to a distinct form of catastrophic cell death we term cytothripsis. Such defects arise during lymphocyte migration in collagen-dense tissues when DOCK8, through CDC42 and p21-activated kinase (PAK), is unavailable to coordinate cytoskeletal structures. Cytothripsis of DOCK8-deficient cells prevents the generation of long-lived skin-resident memory CD8 T cells, which in turn impairs control of herpesvirus skin infections. Our results establish that DOCK8-regulated shape integrity of lymphocytes prevents cytothripsis and promotes antiviral immunity in the skin.

DOCK8, which is highly expressed only within the immune system, functions as an atypical guanine nucleotide exchange factor (GEF) to activate small Rho GTPases (Côté and Vuori, 2002; Ruusala and Aspenström, 2004; Meller et al., 2005; Harada et al., 2012; Mou et al., 2012) and its role as an adaptor in TLR9-MYD88 signaling suggests additional functions beyond GEF activity (Jabara et al., 2012). DOCK proteins and their orthologs participate in diverse biological processes, including gonadal and epidermal cell migration during embryonic development, tumor cell invasion, and leukocyte chemotaxis and trafficking through LNs (Kunisaki et al., 2006; Côté and Vuori, 2007; Gotoh et al., 2008; Kikuchi et al., 2008; Nishikimi et al., 2009, 2013; Harada et al., 2012).

For most people without any obvious immune deficiency, infections with HSV, varicella-zoster virus, or human papillomavirus cause self-limited cold sores, chickenpox, or warts. However, these viruses can reemerge from latency to cause disease in up to ~30% of the population (Higgins et al., 1993; Kilkenny and Marks, 1996; Harpaz et al., 2008). In contrast to normal individuals, DOCK8-deficient patients with autosomal-recessive loss-of-function mutations in *DOCK8* have impaired cellular and humoral immunity (Engelhardt et al., 2009; Zhang et al., 2009; Su et al., 2011; Jing et al., 2014) that manifests as extreme susceptibility to skin and other infections (Chu et al., 2012). Patients often suffer from disseminated and persistent viral skin infections including those caused by HSV, varicella-zoster virus, human papillomavirus, and molluscum contagiosum. Their chronic viral infections may reflect multiple defects that affect T cell activation, proliferation, survival, and priming by dendritic cells (Zhang et al., 2009; Lambe et al., 2011; Randall et al., 2011; Harada et al., 2012; Crawford et al., 2013), NK cell cytotoxicity (Ham et al.,

*C.G. Dove and J.L. Hor contributed equally to this paper.

The Journal of Experimental Medicine
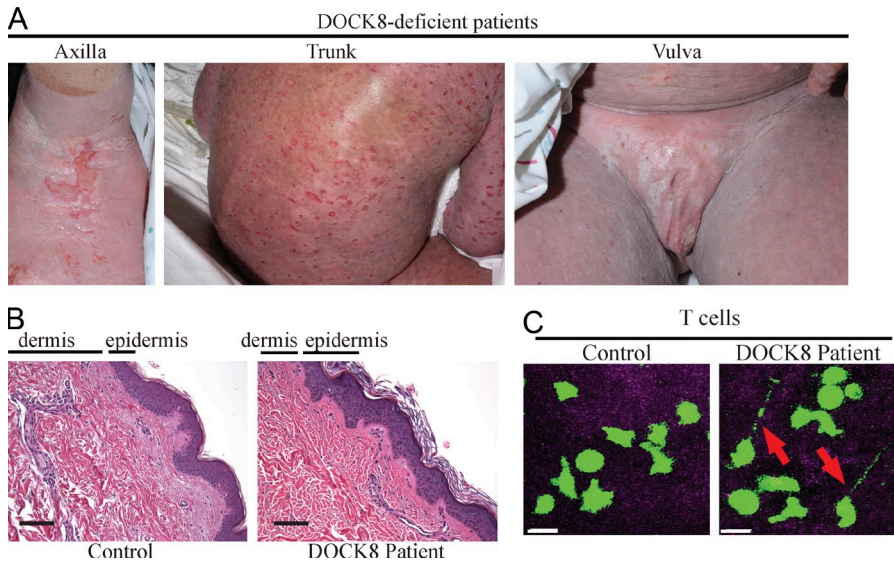
Figure 1. Skin disease in DOCK8–deficient patients. (A) Chronic ulcerating and disseminated HSV infections of the skin involving axilla (left), trunk (middle), and vulva (right) of a DOCK8-deficient patient. 19 of 34 patients in the NIH cohort had similar recurrent or disseminated HSV skin infections. (B) Skin histology in human DOCK8 deficiency. Hematoxylin and eosin staining showing epidermal and dermal layers of skin biopsies from normal healthy control (left) and DOCK8-deficient patient (right). Note highly packed, multilayered epithelial cells in the epidermis and many large pink collagen bundles in the dermis. Bars, 1 mm. Skin biopsies were evaluated from 17 DOCK8-deficient patients. (C) T cells (green) from either a healthy control (left) or DOCK8-deficient patient (right), shown migrating in dermis (purple) of foreskin tissues from healthy donors. Red arrows, elongated cell processes. Bars, 10 µm. Shown is a representative of four patients and four healthy controls tested in three experiments.

2013; Mizesko et al., 2013), and antiviral cytokine production (Zhang et al., 2009).
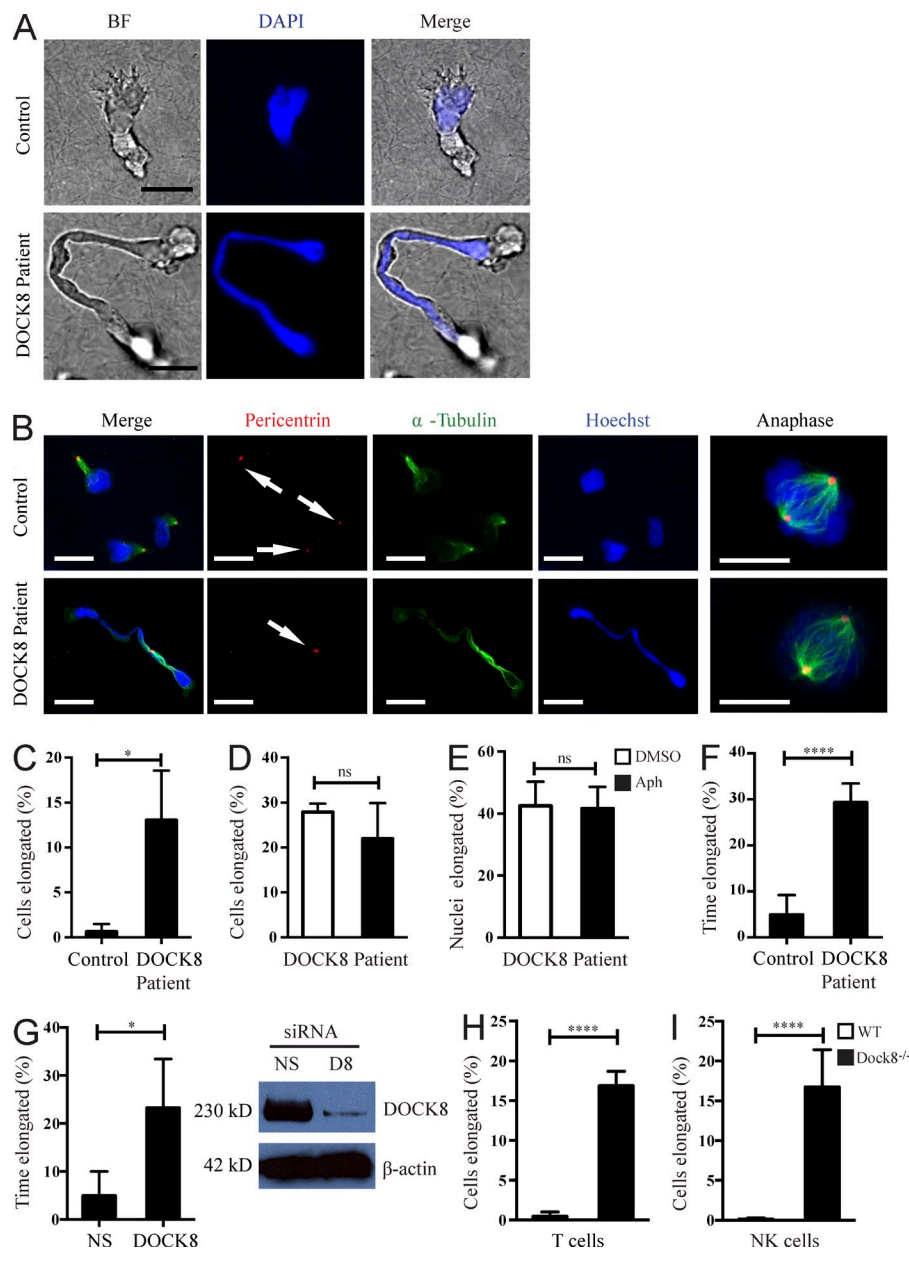
T effector cells are a critical component of immunity to the types of viral skin infections characteristically seen in DOCK8 deficiency. These cells must scan for and target pathogens within the large volume of the skin, which is organized into two layers. The epidermis is composed of interlocking arrays of keratinocytes that impede the passage of immune effector cells (Honda et al., 2014). In contrast, the dermis is composed of a dense network of packed collagen fibers, through which immune cells must navigate (Wolf et al., 2009; Honda et al., 2014). The collagen fibers make up as much as one third of the wet weight of skin, as compared with ∼10% of aorta or ∼1% or less of other organs such as spleen and brain (Lowry et al., 1941; Neuman and Logan, 1950). Thus, the extracellular environments of the epidermis and dermis are characterized by many highly confined spaces, which are likely to tax the structural integrity of cells navigating to their targets. Given the presumptive role of DOCK8 in controlling cell cytoskeletal function and migration capacity, the fact that DOCK8-deficient patients—in comparison with other combined immunodeficiency patients—seem to suffer disproportionately from a broad variety of skin infections, and the evidence for physical constraints on immune cell movement in skin, we investigated whether the skin viral susceptibility of these patients might relate to a defect in effector cell migration. Our studies revealed an unexpected, critical role for DOCK8 in maintaining lymphocyte cellular integrity during migration in dense environments that limits host resistance.

RESULTS

DOCK8–deficient T cells and NK cells develop abnormally elongated shape and nuclear deformation

Despite their susceptibility to skin infections including HSV (Fig. 1 A), DOCK8-deficient patients have histologically normal skin structures (Fig. 1 B), likely reflecting the fact that DOCK8 is not expressed by normal keratinocytes, fibroblasts, and endothelial cells (Su et al., 2011). Dock8-deficient dendritic cells migrate poorly into LNs (Harada et al., 2012). This raised the possibility that impaired presentation of viral antigens by dendritic cells within draining LNs might lead to defective T cell immunity to viruses that infect the skin. However, given that DOCK8 is expressed in T cells as well as myeloid cells, it was also possible that a similar migration defect among skin-infiltrating cytotoxic lymphocytes might impair their effective ability to control viral replication locally. To investigate the motility of DOCK8-deficient T cells, we examined fluorescently labeled T cells from patients that were allowed to migrate into the dermal layer of human foreskin biopsies. The mutant T cells moved through the extracellular matrix of the skin but had abnormally elongated thin processes (Fig. 1 C). A similar phenotype was observed when the skin's dermal layer was modeled in vitro by placing patient T cells into a three-dimensional (3D) collagen gel matrix (Fig. 2 A; and Video 1); this differed from the rounded, nonmotile phenotype reported for Dock8-deficient dendritic cells (Harada et al., 2012). The elongated T cells also had dramatically elongated nuclei (Fig. 2 A). Such elongation was not due to failed cytokinesis despite a role of some DOCK proteins in promoting cell division (Kittler et al., 2007) because elongated cells only had one centrosome (Fig. 2 B), elongation persisted at high levels when cell cycle progression was minimal after prolonged culture (Fig. 2 C), and cell cycle arrest at G1/S did not prevent elongation (Fig. 2, D and E). Time-lapse video microscopy revealed that T cells from patients (Fig. 2 F) spent an increased proportion of time elongated, as did normal T cells in which DOCK8 expression was silenced by transfection with siRNA (Fig. 2 G). Abnormal elongation also occurred in T cells and NK cells from Dock8 mutant mice (Fig. 2, H and I; and Video 2). Like T cells, NK cells are present in the skin of healthy

Figure 2. Abnormal morphology of DOCK8-deficient lymphocytes when migrating in 3D collagen gel matrices.
(A) Confocal imaging of T cells migrating in a collagen gel matrix (3.6 mg/ml) with nuclear staining. BF, brightfield. DAPI, blue. Representative of six experiments. (B) Confocal imaging after in-gel immunofluorescence staining of control and patient T cells for pericentrin (red, indicated by arrows), α-tubulin (green), and nuclei (blue). Stained gels were physically compressed before imaging. Left panels: migrating cells, each showing one centrosome. Right panels: dividing anaphase cells, each showing two centrosomes. Representative of three patients and three healthy controls from three experiments. (C) Proportions of resting T cells that were abnormally elongated. Less than 2% of cells were in S/G2/M phases after 6 wk of culture. Three controls and three patients were tested from three experiments. (D) Proportions of patient T cells that were abnormally elongated after cell cycle blockade. Similar analysis as for C, except that cells were from three patients that were treated with either aphidicolin (Aph) or vehicle (DMSO), tested in three experiments. (E) Nuclear elongation among abnormally elongated cells. Nuclei in cells from D were stained with Hoechst for analysis. (F) Percentage of time cells spent elongated in the collagen matrices. 6 patients and 12 healthy controls were tested from five experiments. (G) Similar analysis as for F, except performed with T cells transfected with *DOCK8* or nonspecific (NS) siRNA, from four experiments. Representative immunoblot showing DOCK8 knockdown efficiency. (H and I) Proportions elongated of T cells (H) and NK cells (I) from 10 Dock8-deficient (KO) or control (WT) mice from three experiments, migrating in collagen gel matrices. Bars, 10 µm. C–I show means ± SD. Unpaired two-tailed Student's *t* test were performed. Statistical significance indicated by *, P < 0.05; ****, P < 0.0001; ns, not significant.

persons and those with inflammatory skin conditions (Ebert et al., 2006; Grégoire et al., 2007). These lymphocytes also help protect against HSV and other viral infections, especially at early times after infection (Biron et al., 1999). Thus, the inability to maintain shape integrity during migration in the 3D microenvironment was an intrinsic property of the lymphocytes due to the lack of DOCK8 expression.

DOCK8-deficient cells exhibit normal chemotaxis but undergo fragmentation and cell death in 3D conditions

The random migratory pattern of T cells within collagen gel matrices mimics their migration pattern in skin tissues, facilitating surveillance for infected cells. We saw that DOCK8-deficient T cells migrating within 3D collagen gel matrices

occasionally remained in place while moving both ends in a poorly coordinated manner, suggesting that immune surveillance could potentially be compromised (Video 1). However, during skin infection, various chemokines are induced (Stock et al., 2014), which could contribute to directed T cell migration toward viral pathogens. To test whether the abnormal morphology of Dock8-deficient T cells was associated with impaired chemotaxis, we tracked individual cells moving through collagen matrices toward a gradient of CXCL12 (SDF-1α). For each cell, directional velocity and track straightness toward the chemokine, as well as speed along the path traveled and track straightness from origin to destination, were analyzed over a 30-min period (Fig. 3 E). The mean values for the population of cells from each DOCK8-deficient patient were similar to
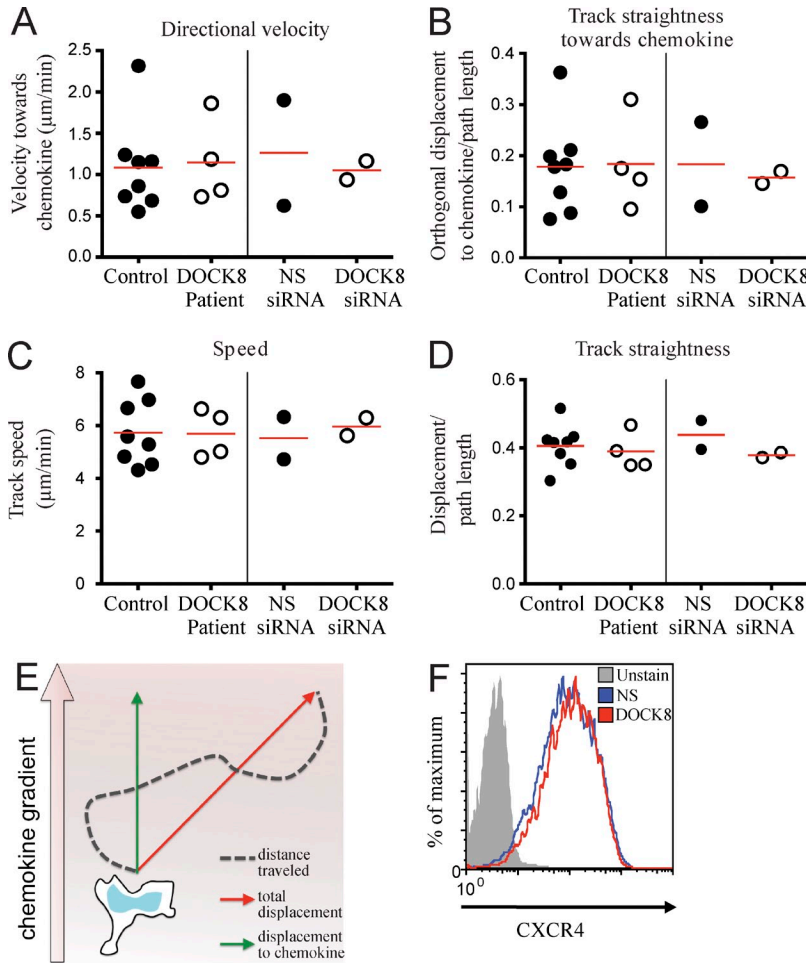
Figure 3. Chemotaxis of DOCK8-deficient T cells migrating toward CXCL12 in collagen gel matrices. (A–D) Velocity toward chemokine (A), chemokine directionality (B), track speed (C), and directionality (D). Each symbol represents the means of these values for individually tracked cells from each sample. The horizontal line designates the average of these means. T cells from four patients and eight controls were evaluated from four experiments. In two separate experiments, normal T cells were transfected with *DOCK8* siRNA or nonspecific (NS) siRNA. (E) Cartoon showing measurements of chemotaxis, based upon the actual route that a cell took as indicated by the gray dotted line. (F) Representative flow cytometric measurement of CXCR4 (receptor for CXCL12) expression on cells used in the chemotaxis assays. Unpaired two-tailed Student's *t* tests were performed. All statistical comparisons were nonsignificant.

normal healthy control cells (Fig. 3, A–D). Chemotaxis was also unaffected when tested using normal T cells in which DOCK8 expression was silenced after transfection with siRNA (Fig. 3, A–D, and F). Thus, DOCK8-deficient cells were capable of normally sensing and migrating toward a chemokine source.

In contrast, after hours of moving within the matrix, patient T cells often fragmented catastrophically as they moved in place (Fig. 4 A and Video 3). The cell fragments contained pieces of deformed nucleus, as shown by propidium iodide (PI) staining. Flow cytometric quantification of dead and dying cells revealed that silencing DOCK8 in otherwise healthy donor human T cells caused them to die within the gels but not within liquid medium (Fig. 4 B). T cells and NK cells, from patients or mice genetically deficient in DOCK8, showed a similar fate (Fig. 4 C and not depicted). Cells that died had spent slightly greater proportion of time elongated, but the duration of elongation episodes immediately preceding fragmentation were longer, suggesting that abnormal morphology correlated with cell death (Fig. 4, D and E). The dying cells recovered from collagen gels showed ultrastructural features reminiscent of apoptosis and necrosis with cell shrinkage, loss of microvilli but no membrane blebbing, and holes in the plasma membrane (Fig. 5 A) but lacked biochemical evidence of classical

apoptosis such as loss of mitochondrial membrane potential or caspase activation (Fig. 5, B–E). This cell death was not blocked by treatment with the pan–caspase inhibitor zVAD-fmk (Fig. 5 F). Together, these results establish that DOCK8-deficient lymphocytes, when moving for prolonged periods in a 3D environment, undergo a distinct form of cell death associated with abnormal cell shape and movement, which we term cytothripsis (cell shattering).

Abnormal elongation requires movement through confined spaces but not adhesive forces

We next investigated the spatial configuration of the microenvironment that elicited this abnormal phenotype. Lowering the concentration of collagen within the gel matrices, which increases the average pore size through which the cells migrate (Pedersen and Swartz, 2005), resulted in a corresponding decrease in the amount of cell death (Fig. 6 A). Abnormal elongation with nuclear deformation also occurred when patient T cells migrated through the small pores of an uncoated polycarbonate transwell insert (Fig. 6 B) or within 3D matrices composed of agarose (Fig. 6 C). This phenotype was not observed when cells moved on ICAM-coated (Fig. 6 D) or
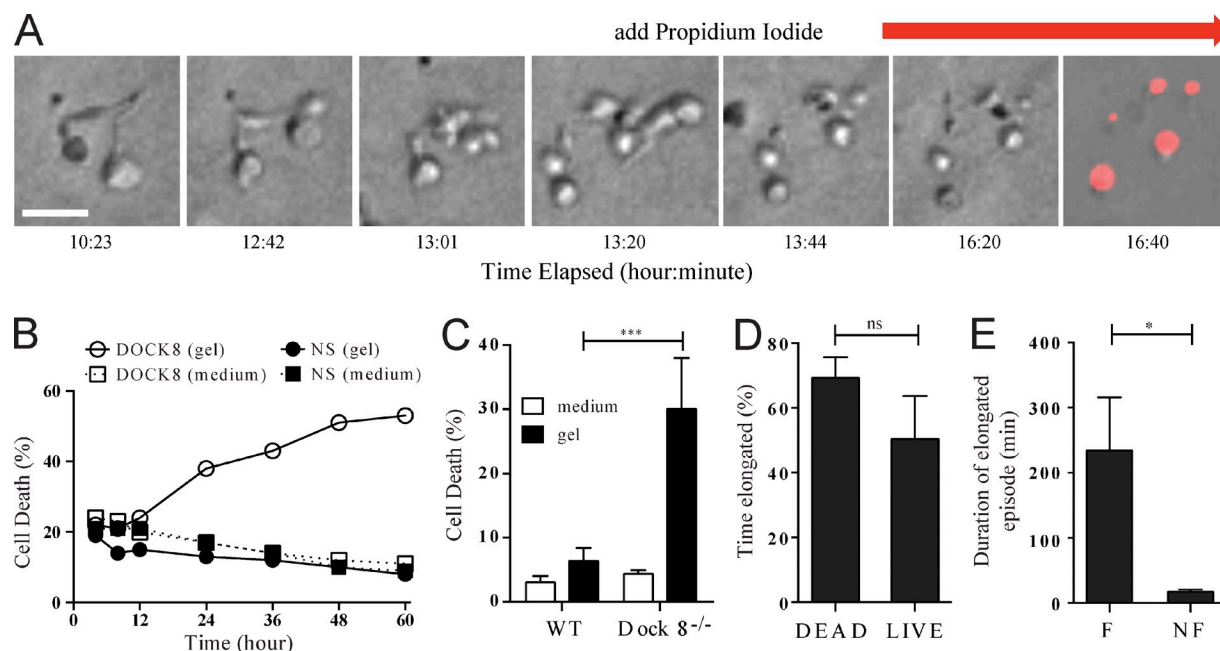
Figure 4. Elongation when migrating through confined spaces leads to cytothripsis. (A) Time-lapse microscopy of a T cell from a DOCK8-deficient patient migrating in collagen matrix. PI (orange) added when indicated. Shown is a representative of three patients and three healthy controls, from three experiments. (B) Flow cytometric quantification of dead and dying cells by Annexin V and PI staining, after collagenase treatment to recover unstained cells. Normal human T cells were transfected with either *DOCK8* (open symbols) or nonspecific (NS) siRNA (filled symbols), and allowed to migrate in collagen matrices (solid line) or medium (dotted line) for the indicated times. Shown is a representative of three experiments. (C) Similar analysis as for B, after migration in medium or collagen for 24 h, of NK cells from six Dock8-deficient (KO) or control (WT) mice from three experiments. (D) Percentages of time spent elongated, for those Dock8-deficient T cells that died or remained alive after migrating in collagen matrix for 16 h. (E) Similar to D, except that duration of elongation episodes was measured for each single episode of elongation that immediately preceded the cell fragmenting (F), or for all other elongation episodes (NF). Bar, 20 µm. Three patients were tested in D and E from three experiments. C–E show means ± SD. Two-way ANOVA was performed for C. Unpaired Student's t test was performed for D and E. Statistical significance indicated by *, $P < 0.05$; ***, $P < 0.001$; ns, nonsignificant.

collagen–coated 2D (Fig. 6 E) flat surfaces. Although integrin-mediated strong adhesive forces are not normally required for leukocyte locomotion within a 3D environment (Lämmermann et al., 2008), the sometimes tethered appearance of elongated DOCK8-deficient cells (Video 1) raised the question of whether such adhesion contributed to the abnormal phenotype. However, this explanation seemed unlikely because agarose and polycarbonate are not ligands for integrin receptors yet could elicit the abnormal phenotype (Fig. 6, B and C). Elongation was also unaffected by disrupting interactions between integrin β1 collagen receptors on patient cells with collagen–containing gel matrix by either adding anti–integrin β1 subunit antibodies to the collagen gel matrix (Fig. 6 E) or silencing its expression within T cells from a DOCK8-deficient patient (Fig. 6 F). Together, these results argue that the abnormal shape integrity of DOCK8-deficient cells was elicited solely by the confined spaces that constrained cell movement. This could explain why the cellular phenotype could vary from tissue to tissue in the body, depending on their physical characteristics, and why disease in the patients manifests as an immunodeficiency with disproportionate involvement of skin, whose tight adhesive junctions between epidermal cells and tight spacing between dermal collagen bands demand marked lymphocyte shape deformation for effective migration.

DOCK8, through CDC42 and p21–activated kinase (PAK), regulates lymphocyte shape integrity to coordinate cytoskeletal structures during cell movement

Lymphocyte migration in the skin presents a challenge especially for the nucleus, which is normally the largest and least deformable organelle (Friedl et al., 2011). Cell body shape change must at some level be coordinated with nuclear shape change during cell migration. Given the elongation phenotype of DOCK8-deficient cells described above, DOCK8 likely regulates this architectural machinery. The small Rho GTPases CDC42 and RAC serve as molecular switches to control diverse biological processes, including cell morphogenesis and migration (Jaffe and Hall, 2005); moreover, DOCK8 can activate CDC42 and RAC (Harada et al., 2012; Mou et al., 2012), regulating CDC42 to facilitate dendritic cell migration (Harada et al., 2012). We therefore investigated the possible contribution of these small GTPases to the DOCK8-deficient phenotype of lymphocytes. Knockdown of CDC42 but not RAC1/2 in T cells from normal donors recapitulated the DOCK8-deficient phenotype of cell elongation, nuclear deformation, and cell death (Fig. 7, A–C). CDC42 in turn activates multiple effectors, including PAK and Wiskott-Aldrich syndrome protein (WASP). Treatment of normal T cells with the class I PAK small molecule kinase inhibitor IPA3, or with
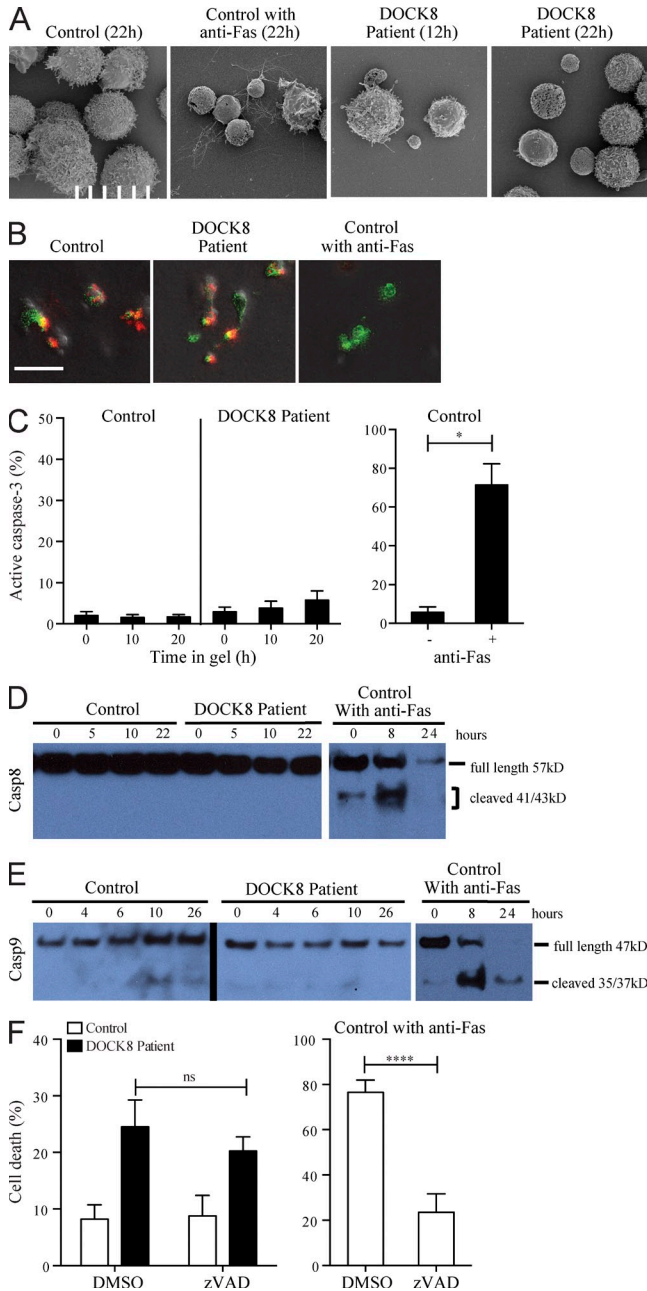
Figure 5. Cytothripsis is biochemically distinct from apoptosis.
(A) Scanning electron micrographs of control or patient T cells after migrating in collagen gel matrices. (B) Mitochondrial membrane potentials of patient or control T cells migrating in collagen gels. A decrease in the ratio of red (JC-1 aggregates) to green (JC-1 monomer) is indicative of loss of potential. (C) Proportions of T cells expressing active caspase-3 after migrating in collagen gels for the indicated times. Eight controls and four patients were tested from four experiments. (D and E) Immunoblotting for highly active cleaved caspase-8 (D) and caspase-9 (E) proteins. Lysates were prepared from control or patient T cells that had migrated in medium (0) or collagen gels for the indicated times. The black line shows that intervening lanes were spliced out. (F) Inability to block cytothripsis with the pan-caspase inhibitor zVAD. Annexin V+ or PI+ staining of migrating cells (nine controls, four patients, from four experiments) was quantitated by flow cytometry after recovery of unstained cells from gels

PAK1/2 siRNA, also phenocopied loss of DOCK8 or CDC42 (Fig. 7, D–F), whereas loss of WASP expression in T cells showed no such effect (Fig. 7, G and H). Similar results were seen for T cells from a Wiskott–Aldrich syndrome patient or *Was* KO mice (unpublished data). Loss of DOCK8, CDC42, or PAK1/2 expression or function did not reciprocally decrease each other's protein levels (unpublished data; Akbar et al., 2011). These results suggest that DOCK8 acts proximally with CDC42 and PAK in regulating lymphocyte shape integrity, most likely through complex spatial and temporal effects on actin, myosin, and microtubule cytoskeletal structures (Bokoch, 2003; Li and Gundersen, 2008). Indeed, the absence of DOCK8, CDC42, or PAK activity resulted in cytoskeletal discoordination between the front and rear of migrating cells, seen as abnormal cellular elongation with slightly decreased total F-actin polymerization present at both poles and abnormal positioning of the microtubules including the microtubule organizing center (Fig. 8).

Defective cell integrity occurs during response to viral skin infections

Viral replication in the skin occurs primarily within keratinocytes in the epidermis; however, some viruses also infect dermal cells such as fibroblasts or neurons at the epidermal–dermal junction (Cunningham et al., 1985; Drijkoningen et al., 1988; Muraki et al., 1992; Nikkels et al., 1996). This places special demands on effector immune cells that must successfully navigate into and through dermis after exiting dermal vessels and then migrate further into the densely connected cell layers of the epidermis to mediate host defense. To assess the function of Dock8-deficient T cells during a viral infection, we infected mice with HSV, which is the only virus causing severe skin infection in patients that is also capable of infecting mice. When HSV is inoculated in the epidermis on the flank, it establishes infection within the dorsal root ganglion before spreading through the nerves, from which it emerges to cause a skin rash in a dermatomal distribution (Fig. 9 A; Simmons and Nash, 1984). Containment of the rash reflects the ability of CD8 T cells to limit secondary spread of the virus down the flank (van Lint et al., 2004). Upon acute infection, Dock8-deficient mice developed herpetic skin disease that was more severe with increased mortality when compared with WT mice (Fig. 9, A–C). To visualize T cells that were responding within the infected skin, we adoptively transferred Dock8-deficient or control WT T cells into normal mice. The recipient mice were

with collagenase. All panels show a positive control in which apoptosis was induced in healthy donor T cells within the collagen gels using anti-FAS antibodies with Protein A cross-linking. Cells were analyzed after migrating within the collagen gels for the indicated times or as described in the Materials and methods. A, B, D, and E show representatives of three tested patients and controls from three experiments. Bars, 10 µm. C and F show means ± SD. Unpaired Student's *t* test was performed for C and F (right), and two-way ANOVA was performed for F (left). Statistical significance indicated by *, P < 0.05; ****, P < 0.0001; ns, nonsignificant.
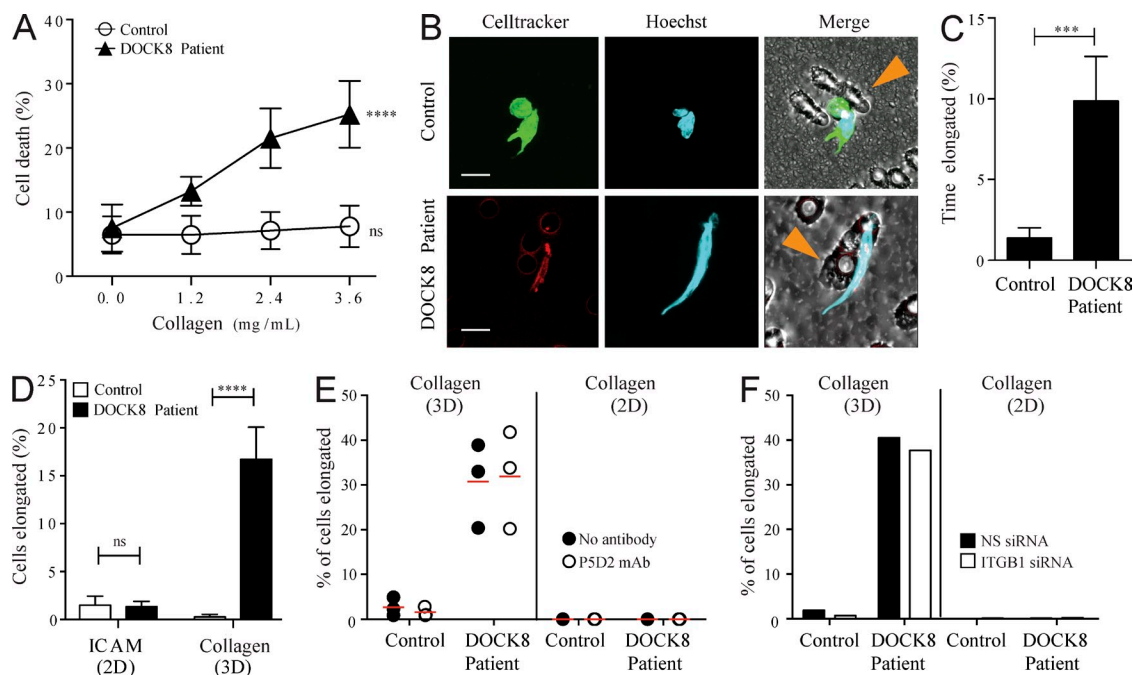
Figure 6. Requirement for migration through confined spaces but not for adhesion in eliciting loss of shape integrity. (A) Proportions of T cells (nine controls, four patients, from four experiments) that were Annexin V$^+$ or PI$^+$, after migration in increasing collagen concentrations for 24 h in collagen gels of increasing matrix density. (B) Confocal and diffusion interference contrast (DIC) microscopy of control (green) and patient (red) T cells while migrating through transwell pores (orange arrowheads) toward CXCL12. Hoechst, blue. Representative of three patients and three controls from three experiments. (C) Percentage of time T cells (six controls, three patients, from three experiments) spent elongated in 0.2% agarose gel matrices. (D) Proportions of T cells (eight controls, four patients, from three experiments) elongated during migration on 2D ICAM-coated plates or in 3D collagen matrices. (E) Proportions of DOCK8-deficient T cells elongated after migration on collagen-coated slides (2D) or in collagen gels (3D), untreated or with anti–integrin β1 blocking antibodies. Means are shown for three patients and three controls tested under each condition from three experiments. Two-way ANOVA was performed to compare treatment with or without antibody. (F) Similar to E except that one patient and one control were tested after transfection of nonspecific or *ITGB1* siRNA. Median fluorescence intensities of CD29 for control cells were 6,386 (NS siRNA) and 2,019 (*ITGB1* siRNA), and for patient cells were 6,363 (NS siRNA) and 1,396 (*ITGB1* siRNA). Bars, 10 µm. A, C, and D show means ± SD. Linear mixed effects modeling was performed for A, unpaired two-tailed Student's *t* test for C and D, and two-way ANOVA to compare treatment with or without antibody for E. Statistical significance indicated by ***, P < 0.001; ****, P < 0.0001; ns, nonsignificant.

infected epicutaneously with HSV, and the donor T cells were visualized in the skin using intravital two-photon microscopy (Gebhardt et al., 2011). In contrast to normal T cells, responding Dock8-deficient T cells showed increased elongation and fragmentation as they migrated within the combined epidermal and dermal layers, indicating that DOCK8 regulates cell shape integrity in vivo (Fig. 9, D and E; and Video 4).

DOCK8 regulates skin tissue–resident memory cell formation for protection against viral infection

During HSV infection, control of replicating virus requires a high density of CD8 T cells, which migrate into the epidermis and develop into tissue-resident memory CD8 T cells (T$_{RM}$ cells; Gebhardt et al., 2009; Zhu et al., 2013). These cells persist indefinitely after acute inflammation resolves within the epidermis, where they continuously migrate to protect against viral reinfection or emergence from latent infection in the skin (Gebhardt et al., 2011; Ariotti et al., 2012; Jiang et al., 2012; Mackay et al., 2012; Mueller et al., 2013; Zaid et al., 2014). In the epidermis, T$_{RM}$ cells adopt a highly ramified cell shape that is defined by the constraints of the tissue through which

they migrate (Zaid et al., 2014). Thus, we hypothesized that cytothripsis, associated with defective shape integrity, could impair the formation or survival of epidermal T$_{RM}$. This would decrease the effective virus-specific T cell concentration below that needed for viral clearance, despite substantial remaining cytotoxic activity and cytokine production during the immune response (Zhang et al., 2009; Lambe et al., 2011; Randall et al., 2011). Other infected organs and normal secondary lymphoid tissue, in contrast, would offer a less confined environment for cell migration and reduce these damaging effects on anti-pathogen immune cells. To test this, normal mice were transferred with equal mixtures of Dock8-deficient and control WT T cells, both also expressing the same transgenic TCR that recognizes an MHC class I–restricted immunodominant HSV peptide (Mueller et al., 2002). After epicutaneous infection, Dock8-deficient effector T cells expanded and accumulated in secondary lymphoid organs and skin with only slightly reduced efficiencies as compared with control T cells (Fig. 10 A). Consistent with previous reports that Dock8-deficient CD8 T cells had reduced long-term survival (Lambe et al., 2011; Randall et al., 2011), these cells were disproportionately
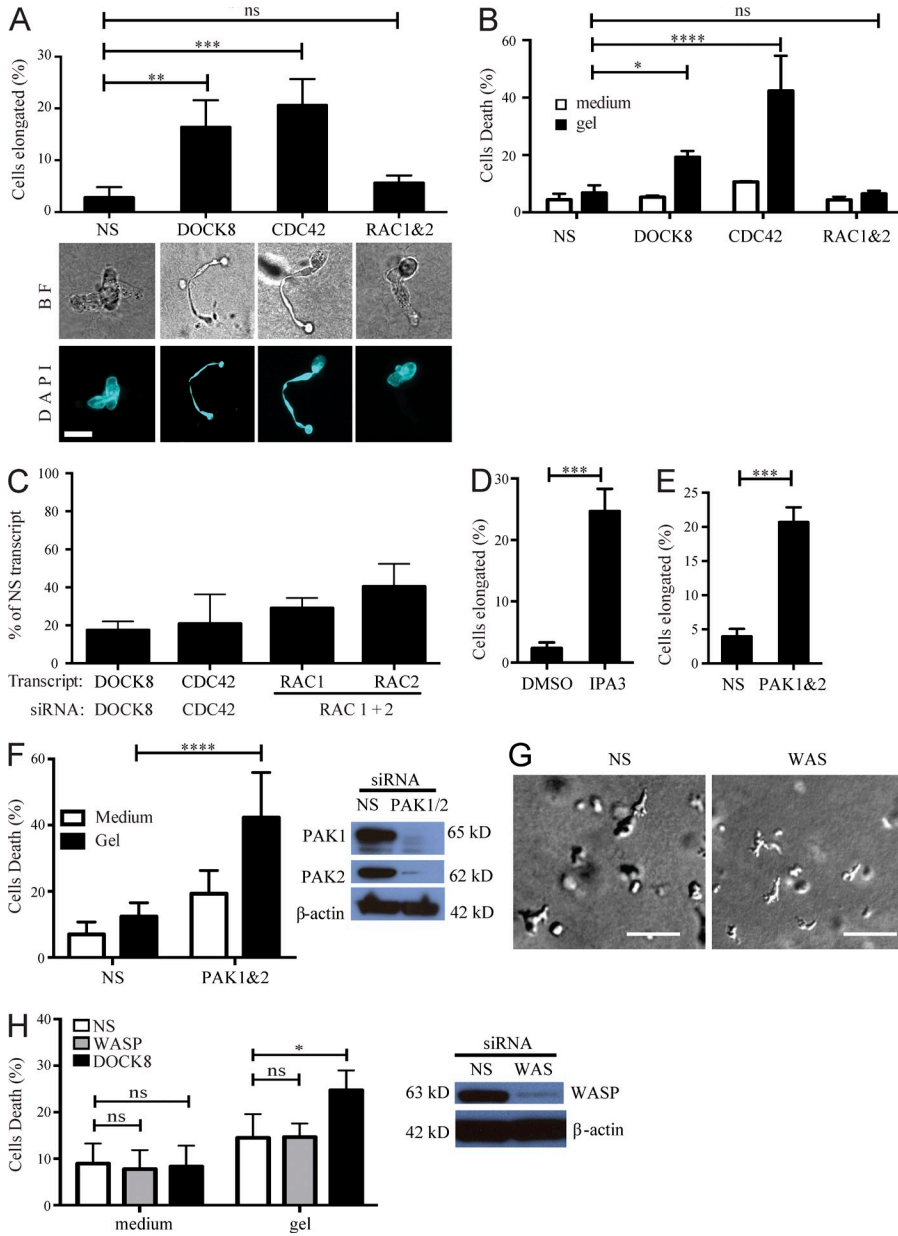
Figure 7. DOCK8 signals through CDC42 and PAK to maintain shape integrity.
(A) Top: Proportions of T cells elongated during migration in collagen gel matrices. Normal human T cells were transfected with nonspecific (NS), *DOCK8*, *CDC42*, or *RAC1/2* siRNA. Bottom: representative nuclear morphology of these cells migrating in collagen gels. BF, brightfield. DAPI, blue. (B) Proportions of dead or dying cells were quantitated by flow cytometric analysis of Annexin V and PI staining, after cells from A were allowed to migrate in collagen gels or in medium. (C) Knockdown efficiencies for A and B. Quantitative real-time RT-PCR to measure transcript levels of *DOCK8*, *CDC42*, *RAC1*, and *RAC2*, normalized to β-actin. Knockdown efficiencies of these genes were calculated as normalized levels in T cells transfected with indicated siRNA, divided by normalized levels in T cells transfected with nonspecific siRNA. Ratios are means ± SD of five independent experiments. (D and E) Proportions elongated within collagen gels of normal human T cells either treated with DMSO or the PAK inhibitor IPA3 (D), or transfected with NS or *PAK1/2* siRNA (E). (F) Similar analysis as in B, using cells from E. Representative immunoblot showing efficiency of PAK1/2 knockdown. (G) Morphology of T cells in which *WAS* gene expression was silenced, during migration in collagen gel. (H) Proportions of Annexin V[+] or PI^{+} cells, after migrating in collagen gel matrices or medium. Normal human T cells were transfected with NS, *WAS*, or *DOCK8* siRNA. Representative immunoblot showing WASP knockdown efficiency in human T cells. Bars, 10 µm. A, B, D, E, G, and H are representative of three independent experiments, and F of five experiments. A–F and H show means ± SD. One-way ANOVA was performed for A, two-way ANOVA for B, F, and H, and unpaired two-tailed Student's *t* test for D and E. Statistical significance indicated by *, $P < 0.05$; **, $P < 0.01$; ***, $P < 0.001$; ****, $P < 0.0001$; ns, nonsignificant.

decreased in the spleens as infection resolved and immunological memory developed (Fig. 10, B and C). However, the survival defect was markedly more pronounced in the skin, where up to 180 times more WT than Dock8-deficient memory T cells were recovered after 1 mo (Fig. 10 B). When we examined the skin in these mice by intravital two-photon microscopy, Dock8-deficient T cells were initially rare but became largely undetectable by 1 mo after infection, despite normal numbers of control T cells (Fig. 10 D and Video 5). This was primarily due to decreased numbers of CD69^{hi} CD103^{+} Dock8-deficient T_RM, which failed to survive in the skin after HSV infection (Fig. 10 E).

To analyze the formation of CD103^{+}CD8^{+} T_RM cells in the skin, we cotransferred in vitro activated effector CD8 T cells from Dock8-deficient or control TCR transgenic mice directly into the skin. This method circumvents any defects in T cell priming and migration to the skin, allowing direct assessment of the ability of the cells to enter the epidermis and develop into T_RM cells (Mackay et al., 2013). Dock8-deficient T cells rapidly disappeared in the skin and the few surviving cells did not up-regulate expression of CD69 and CD103, which are necessary for T_RM formation (Fig. 10, F and G). Defective T_RM survival with severe loss of cells over time resulted in minimal protection against challenge with HSV, as measured by viral titers in the skin (Fig. 10 H) after transfer of effector T cells and topical treatment of recipient mice with the chemical sensitizer 2,4-dinitrofluorobenzene (DNFB) to generate T_RM (Mackay et al., 2012). Together, these results
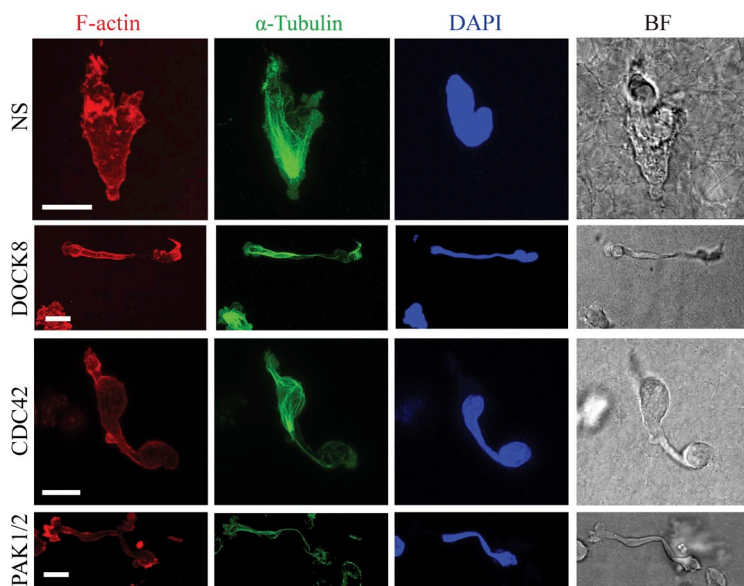
Figure 8. Abnormal cytoskeletal organization in elongated cells. In-gel confocal imaging for F-actin (phalloidin, red), α-tubulin (green), and nuclei (DAPI, blue), in normal human T cells transfected with nonspecific (NS), *DOCK8*, or *CDC42* siRNA, or treated with the PAK1/2 inhibitor IPA3. Representative of three experiments. Bars, 10 μm.

indicate that DOCK8, by regulating cell shape integrity, is critical in vivo for CD8 T cell persistence, T_{RM} formation, and antiviral immunity in the skin.

DISCUSSION

While studying the behavior of DOCK8-deficient T cells and NK cells, we have unexpectedly discovered a new form of cell death we term cytothripsis for "cell shattering." Cytothripsis occurs when shape maintenance fails during lymphocyte migration. This process can be elicited by the physical properties of tissues through which the cells migrate, and it is characterized by cell elongation and nuclear deformation during prolonged migration through confined spaces. The resulting mechanical forces experienced by the cell likely cause breaks in the plasma membrane and nucleus that lead to catastrophic cell death without inducing any biochemical markers of apoptosis. Cytothripsis can impair effector T cell and NK cell functions by limiting their effective motility and decreasing their
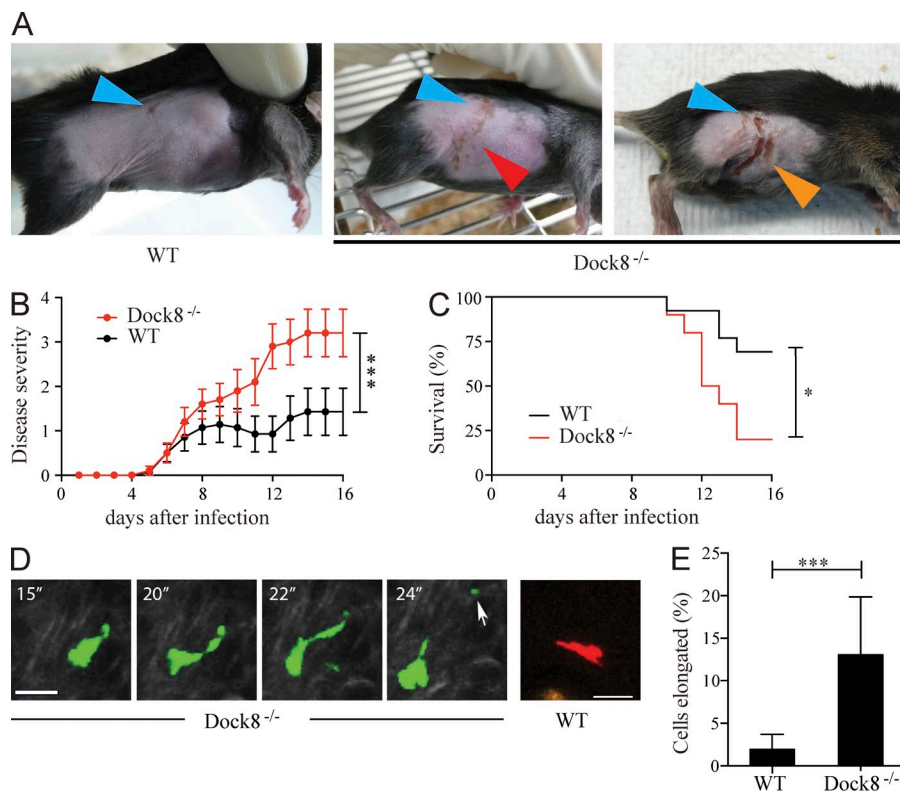
Figure 9. Defective cell integrity occurs during response to viral skin infections. (A) Representative skin disease, 7 d after epicutaneous HSV infection of WT or Dock8-deficient (KO) mice. Blue arrowheads, primary infection sites. Red arrowhead, blistering along infected dermatome. Orange arrowhead, blistering with skin necrosis. (B) Daily scoring of disease severity after acute HSV infection of WT (black) or KO (red) mice. (C) Kaplan-Meier survival curves for the mice from (B). (D) Two-photon imaging of Dock8-deficient cpm (green) or Dock8-replete T cells from WT gBT-I mice (red) migrating in the dermis, 7 d after adoptive cotransfer into WT recipient mice and HSV infection. White arrow, fragmentation. Frames show time elapsed (minutes). (E) Proportions elongated of the cotransferred T cells in D. Bars, 15 μm. B shows means ± SEM, with a total of 10 or 14 mice per group from two experiments. E shows means ± SD, where data were pooled from six mice from two experiments. Wilcoxon matched-pairs signed rank sum test (two-tailed) was performed for B, log-rank (Mantel-Cox) test for C, unpaired two-tailed Student's *t* test for E. Statistical significance indicated by *, P < 0.05; ***, P < 0.001.
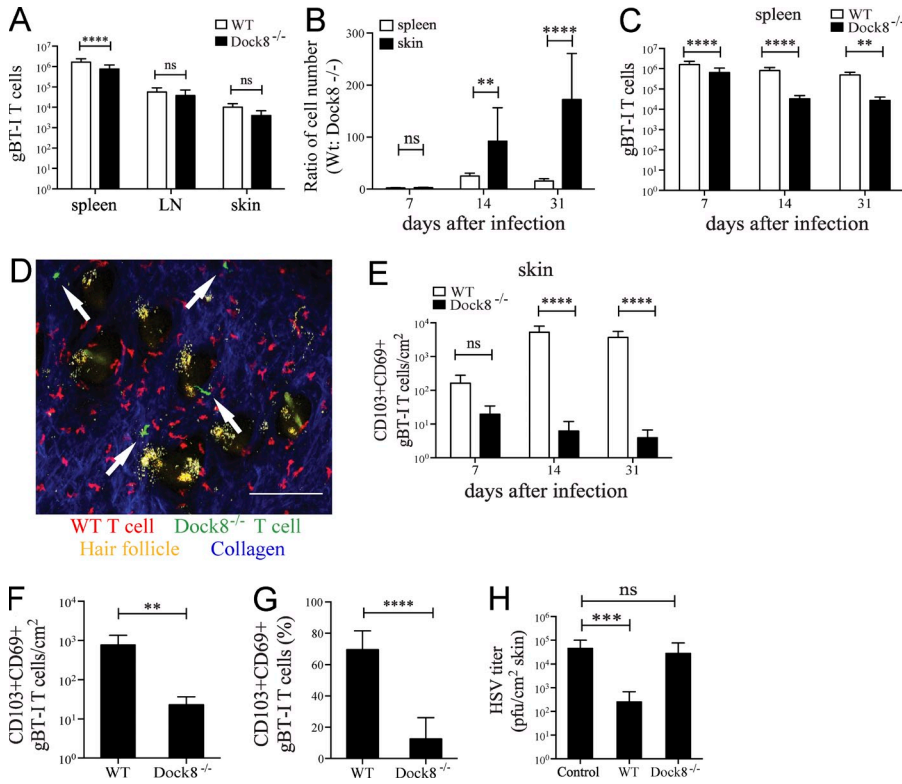
Figure 10. Dock8 regulates shape integrity and survival of T$_{RM}$ cells in vivo to control viral skin disease. (A) Numbers of WT and Dock8-deficient HSV-specific gBT-I T cells in the spleen, brachial LNs and skin, 7 d after adoptive transfer (1:1 mixture) into WT recipient mice and HSV infection. (B) Relative numbers of WT gBT-I and Dock8-deficient cpm gBT-I T cells in spleen and infected skin, quantified by flow cytometry at the indicated times after infection. (C) Numbers of WT and Dock8-deficient gBT-I T cells in the spleen at various times after skin infection. (D) Two-photon imaging of skin in C on day 17 after infection. White arrows, Dock8-deficient cells. (E) Numbers of WT and Dock8-deficient gBT-I T cells in skin (CD103$^+$ CD69$^+$ T$_{RM}$) in C. (F) Numbers of WT and Dock8-deficient skin (CD103$^+$ CD69$^+$) T$_{RM}$, at 23 d after intradermal cotransfer of in vitro–activated CD8 T cells into WT recipient mice. (G) Proportions of CD103$^+$ CD69$^+$ gBT-I T$_{RM}$ that were WT or Dock8$^{-/-}$ in skin in F. (H) Impaired control of HSV skin infection by virus-specific memory cells. WT mice received no cells (control) or in vitro activated effector CD8 T cells from WT gBT-I or Dock8-deficient cpm gBT-I mice. After topical treatment with DNFB, mice were infected at the same site 30 d later with HSV and viral titers measured on day 5. Bar, 100 µm. A–C and E–H show means ± SD. For A, data were pooled from four experiments with a total of 20 mice per group. For B, C, and E, data were pooled from four experiments for the day 7 and 31 time points and two experiments for the day 14 time point, with a total of 10–20 mice per time point. F and G are representative of three experiments with seven mice per group. For H, data are from three experiments with a total of 13–15 mice per group. Two-way ANOVA was performed for A–C and E, unpaired two-tailed Student's t test for F and G, and one-way ANOVA for H. Statistical significance indicated by **, P < 0.01; ***, P < 0.001; ****, P < 0.001; ns, nonsignificant.

capacity to reach virally infected cells within the tissue in a viable state. Skin is among the densest tissues within the body and therefore most likely to elicit cytothripsis, given that both epidermis and dermis have many highly confined spaces. Although collagen content is a main determinant of tissue density in the dermis (Lowry et al., 1941), other environmental constraints, such as the cellular density and tight junctions in the epidermis, likely also define the migratory capacity of leukocytes in tissues. Tissues of intermediate density, such as the walls of large arteries, may also elicit cytothripsis, thereby contributing to the vasculopathy associated with local virus reactivation that has been documented in some DOCK8-deficient patients (Sabry et al., 2014; unpublished data).

Maintenance of lymphocyte shape integrity, which prevents cytothripsis, is regulated by DOCK8 which, together with CDC42 and PAK, coordinates cytoskeletal structures during cell migration. The demand for precise coordination of cytoskeletal structures is greatest in cells when they maneuver through highly confined spaces, as compared with open spaces. In lymphocytes, coordination of cytoskeletal structures is also required during immune synapse formation for cytotoxicity, directed cytokine secretion, assembly of signaling platforms for activation and proliferation, and cell division (Dustin, 2008). External signals determine which of many

GEFs become stimulated to activate CDC42, as well as which effectors downstream of CDC42 become selectively activated to carry out the different shape rearrangements for these cellular functions (Sinha and Yang, 2008). This could explain why DOCK8- and WAS-deficient cells differ in their migration behavior, and why DOCK8 could contribute not only to the striking migration defects we have now observed but also to the lymphopenia and other functional defects that have been reported in DOCK8-deficient lymphocytes.

Dock8-deficient T cells were previously reported to exhibit a long-term survival defect, as shown by their competitive disadvantage after adoptive transfers of mixtures of mutant and WT cells (Lambe et al., 2011; Randall et al., 2011). Furthermore, fewer memory CD8 T cells persisted in Dock8-deficient mice after experimental influenza virus infections (Lambe et al., 2011; Randall et al., 2011). Our results during experimental HSV skin infections also indicated that Dock8 mutant T cells are at a competitive disadvantage. However, it is unlikely that they would survive better in a noncompetitive situation, or at least not sufficiently to restore function, given that transfer separately of either WT or Dock8 mutant HSV-specific T cells, followed by challenge of mice after establishment of memory, conferred no protection in terms of viral replication. Interestingly, mice conditionally deficient in

Cdc42 also showed increased ex vivo expression of apoptotic markers in their peripheral T cells, which could be rescued in vivo by overexpressing PAK1 (Guo et al., 2010). Although the decreased survival was attributed to small decreases in IL-7 receptor expression for survival signals (Guo et al., 2010; Randall et al., 2011), our results suggest another mechanism whereby survival depends not only upon access to survival signals (unpublished data) but also whether the cell can withstand physical stresses as it migrates through the body. Such stress may have a cumulative effect on trafficking T cells that is pronounced in certain tissues, such as the skin.

The different migratory patterns of T cells allow them to perform their important immunosurveillance functions of preventing reinfection or controlling viral reactivation throughout the body (Mueller et al., 2013). To accomplish this, naive and central memory T cells continually migrate between blood and secondary lymphoid organs, whereas effector memory T cells also migrate through peripheral tissues. When they circulate through skin, effector memory T cells can be found moving rapidly through the dermis en route to draining LNs. In contrast, CD8 memory T cells in the skin do not recirculate throughout the body but instead remain indefinitely within the epidermis where they continuously move. T_{RM} cells also form in other nonlymphoid tissues in response to infections, including the intestines, reproductive tract, and lungs, where they are predominantly associated with epithelial layers (Mueller et al., 2013). Although the ability of Dock8-deficient T cells to form T_{RM} populations in those tissues has yet to be examined, the unique microanatomy of those tissues may differ from the skin in having less confinement, which could facilitate some degree of T_{RM} generation. This would help explain the disproportionate number and severity of viral skin infections in DOCK8-deficient patients. Nevertheless, reduced T_{RM} in the lungs or mucosal surfaces may contribute to the recurrent sinopulmonary infections and chronic anogenital viral infections in DOCK8-deficient patients. Moreover, even during acute infections, T cells may be subjected to physical stresses from the highly confined skin environment. This could lead to the increased morbidity and mortality we saw during epicutaneous HSV infections, in contrast to the normal morbidity previously seen during intranasally inoculated influenza virus infections of Dock8-deficient mice (Lambe et al., 2011).

Collectively, our data are highly suggestive that the abnormal elongation phenotype is responsible for T cell death in vivo and that this process prevents T_{RM} formation during viral infections. However, other explanations, including impaired migration and proliferation or alternative mechanisms of cell death, remain possible. These appear less likely given our results showing normal chemotaxis, impaired T_{RM} formation even when activated T cells were directly transferred to the skin, and normal proliferation and activation of T cells from Dock8-deficient mice (Lambe et al., 2011). Nevertheless, other immunodeficiencies demonstrate that additional mechanisms exist to control viral skin infections. For example, the WHIM syndrome, GATA2 deficiency, or the Wiskott-Aldrich syndrome, which result from impaired chemotaxis, loss of peripheral NK cell and dendritic cell differentiation, and/or defective actin polymerization, can also be associated with viral skin infections, although the skin infections tend to be of narrower spectrum or later onset than DOCK8 deficiency (Sullivan et al., 1994; Imai et al., 2004; Dotta et al., 2011; Sanal et al., 2012; Spinner et al., 2014). Interestingly, in the Wiskott-Aldrich syndrome, the defective actin polymerization affects many T cell functions including thymopoiesis, chemotaxis, activation, proliferation, cytokine production, and cytotoxicity (Zhang et al., 1999; Snapper et al., 2005; De Meester et al., 2010; Lang et al., 2013). However, when compared with DOCK8 deficiency, the lack of abnormal elongation and cytothripsis and less frequent occurrence of recurrent viral skin infections in Wiskott-Aldrich syndrome patients (Sullivan et al., 1994) support the concept that lymphocyte shape integrity contributes to normal protection against viral skin infections.

In summary, our work has now revealed that the ability to maintain cell shape integrity is a critical determinant of immune function in rapidly motile cells such as lymphocytes. Although we have focused on the role of lymphocyte cell shape integrity in antiviral immunity, our findings are likely to have general relevance for skin immunity. For example, DOCK8-deficient patients also often have bacterial or fungal skin infections, and are at increased risk of developing skin cancers. We speculate that these conditions result from locally impaired defense against those pathogens, and possibly impaired tumor surveillance, when lymphocytes undergo cytothripsis as they navigate to lesions in skin tissues. Dock8-deficient dendritic cells also show more globally impaired interstitial migration that might further compromise skin immunity (Harada et al., 2012). Maintenance of lymphocyte shape integrity may also become a factor when cells repeatedly traverse less dense tissues such as blood vessel walls or lymphoid tissues. Because many T cell populations recirculate between blood, lymphatics, and other tissues, our results may mechanistically explain the milder systemic defect in peripheral CD8 memory T cell survival and attrition of naive T cell numbers in DOCK8-deficient humans or mice (Lambe et al., 2011; Randall et al., 2011). Finally, our results suggest a more general conclusion that loss of shape integrity during the navigation of nonimmune cells in other migratory processes, such as during embryonic development, could contribute to human disease.

MATERIALS AND METHODS

Patients. Whole blood and leukapheresis samples were obtained from mutation- and immunoblot-confirmed DOCK8-deficient patients, their relatives, or paid healthy volunteers. Only those patients without somatic reversion or at most ∼25% of revertant T cells (Jing et al., 2014) were used for the studies described here. These individuals gave written informed consent to participate in research protocols approved by National Institutes of Health (NIH) Institutional Review Boards. Buffy coat cells, which were by-products of volunteer-donor blood units, and human foreskin tissues (gift from C. Yee, National Cancer Institute, Bethesda, MD), which were discarded after routine newborn circumcisions, were distributed in an anonymized manner. These were exempted from need for informed consent and Institutional

Review Board review, as determined by the NIH Office of Human Subjects Research Protection.

Mice. Mice were bred and used under animal study protocols approved by the NIAID Animal Care Use Committee, UK Home Office License, and the University of Melbourne Animal Ethics Committee. Dock8-deficient *cpm/cpm* (cpm) mutant mice, generated by ENU mutagenesis from a pure C57BL/6 background, gBT-I TCR transgenic mice recognizing an MHC I–restricted HSV-1 gB epitope, and Actb-DsRed transgenic mice were previously described (Mueller et al., 2002; Vintersten et al., 2004; Randall et al., 2009). To obtain Dock8-deficient GFP-expressing mice (GFP-cpm) for cell tracking experiments, cpm mice were crossed to UBI-GFP transgenic mice on a C56BL/6 background (The Jackson Laboratory; Schaefer et al., 2001). Mice were further crossed with gBT-I TCR transgenic mice to enable assessments of virus-specific T cells. WT gBT-I TCR transgenic mice were crossed to Actb-DsRed transgenic mice for use as controls. In some experiments, Dock8-deficient KO mice were used instead of cpm mice. KO mice were generated from targeted deletion of exons 9 and 10 in pure C57BL/6 ES cells. WT control C57BL/6 mice were purchased from Taconic or The Jackson Laboratory. Mice were sacrificed by carbon dioxide asphyxiation or cervical dislocation for harvest of LNs and spleens.

Cell isolation for in vitro experiments. Human peripheral blood mononuclear cells (PBMCs) were isolated from peripheral blood products by Ficoll-Paque PLUS density gradient centrifugation (GE Healthcare). T cells were purified from PBMC by negative selection using human pan–T cell isolation kit II (Miltenyi Biotec). In some samples, eosinophils were further depleted using human CD15 microbeads (Miltenyi Biotec). T cells were activated using beads coated with anti-CD2, -CD3, and -CD28 antibodies provided as a T cell activation/expansion kit (Miltenyi Biotec), using a bead to cell ratio of 1. Beads were removed on the fourth day after activation, and cells were expanded in 100 U/ml of recombinant human IL-2 (Aldesleukin; Prometheus). Activated T cells were cultured for a total of 4–45 d, when they acquired an activated effector/memory phenotype, as reflected by loss of CD45RA and CCR7 surface marker expression, that was comparable between patients and healthy normal controls. The proportions of revertant cells were determined in one patient, which appeared stable or mildly increased, ranging from 18% on day 2, 14% on day 8, and 26% on day 21 during culture. Human NK cells were purified by positive selection using CD56 microbeads (Miltenyi Biotec) and expanded in 100 U/ml of recombinant human IL-2 for 6–8 d. Human T cells and NK cells were typically >90 and >85% purity, respectively, when used in experiments.

Mouse LNs and spleens were minced into single cell suspensions and passed through a cell strainer. Splenocytes were also treated with ACK lysing buffer (Quality Biological). Mouse LN T cells or splenic NK cells were purified by negative selection, using mouse pan–T cell or NK cell isolation kits II (Miltenyi Biotec). Plates were coated overnight with anti-CD3 and anti-CD28 antibodies (BD) at 3 µg/ml in PBS to which purified pan–T cells were added. After activation for the first 3 d, T cells were expanded in 200 U/ml of recombinant human IL-2. Purified mouse T cells were cultured for a total of 5–7 d. Purified mouse NK cells were activated and expanded with 1,000 U/ml of recombinant human IL-2 for 6–7 d. Mouse T cells and NK cells were typically >90% purity when used in experiments.

Human and mouse cells were grown in complete medium, consisting of RPMI medium supplemented with 10% FBS, ʟ-glutamine, penicillin, streptomycin, and recombinant human IL-2. Unless otherwise indicated, cells were kept in the presence of IL-2 throughout subsequent experiments, including within 3D matrices.

Lymphocyte immunophenotyping. Standard flow cytometry methods were used to evaluate cell surface marker expression using various combinations of FITC, PE, PE-Cy5, PE-Cy7, APC, APC-Cy7–conjugated anti-CD3, anti-CD4, anti-CD16, anti-CD25, anti-CD29, anti-CD45RA, anti-CD56, and PE anti-CXCR4 antibodies (Life Technologies; the rest of the antibodies are from BD). CFSE dilution assays were performed as previously described

(Zhang et al., 2009). Samples were acquired on a FACSCanto instrument using FACSDiva software (BD). Analyses were performed using the FlowJo software version 9 and higher (Tree Star).

Migration studies in human foreskin tissues. Human foreskin tissues discarded after routine newborn circumcisions were stored in HBSS at 4°C for 3–7 d before use. Tissues were warmed to 37°C overnight in PBS supplemented with 10% FBS, cut into 5 × 5 mm pieces, and the epidermis carefully peeled off using a small forceps. T cells, labeled with 0.5 µM Cell-Tracker Green CMFDA (5-chloromethylfluorescein diacetate; Life Technologies), were dropped onto the exposed dermis and allowed to migrate into the tissues at 37°C for 3 h. Cells remaining on the dermal surface were gently rinsed away, and tissues immersed in complete medium within Lab-Tek II 8-well chambered coverglasses (Nunc). Live cell imaging was performed at 37°C in the presence of 5% CO_2, using a TCS SP5 laser scanning confocal microscope (Leica) with excitation at 488 nm. Image stacks were collected with a 4-µm vertical step size at a depth of 40–60 µm. Collagen was visualized by refractive imaging.

RNA interference. Human T cells, 4–7 d after initial activation, were nucleofected using the Lonza 96-well shuttle system according to the manufacturer's optimized protocol. Stealth select prevalidated siRNA against *DOCK8*, *ITGB1*, *CDC42*, *RAC1*, *RAC2*, *PAK1*, *PAK2*, *WAS*, or nonspecific negative control siRNA were used (Life Technologies). To optimize knockdowns, cells were nucleofected 2 d in a row, and the dead cells removed by Ficoll-Paque PLUS gradient centrifugation on the third day. Experiments were performed and lysates harvested to analyze RNA or protein expression on the fourth day after nucleofection. For *PAK1/2* knockdown, cells were nucleofected every other day for four times, the dead cells removed by Ficoll-Paque PLUS gradient centrifugation 1 d later, and used for experiments and evaluation of knockdown efficiency on the second day after the last nucleofection.

Immunoblotting. Immunoblotting for DOCK8 protein and β-actin was performed as previously described (Zhang et al., 2009). For analysis of other proteins, cells were lysed in 2% SDS (50 mM Tris HCl, pH 6.8, 10% glycerol) or 1% NP-40 (1 mM EDTA, 50 mM Hepes, and 150 mM NaCl) containing complete protease inhibitors (Roche). Protein lysates were separated on Nu-PAGE Novex 12% or 4–12% gradient Bis-Tris gels using MOPS SDS or MES running buffers (Life Technologies), followed by wet or semi-dry transfer. Membranes were blocked with 5% blocking grade nonfat milk (Bio-Rad Laboratories) or bløk-CH (Millipore). Antibodies were to caspase-9 (BD); caspase-8 (clone C15; gift from L. Zheng, NIAID, NIH, Bethesda, MD); and PAK1, PAK2, and WASP (Santa Cruz Biotechnology, Inc.).

Quantitative real-time RT-PCR. Total RNA from transfected primary T cells was isolated using the RNeasy mini kit with DNaseI in-column digestion (QIAGEN). 0.9 µg of total RNA was reverse-transcribed with Superscript III first-strand synthesis supermix (Invitrogen). Diluted cDNA was analyzed by quantitative real-time PCR using Power SYBR Green PCR master mix on a 7500 Real Time PCR System (Applied Biosystems). Standard conditions of 40 cycles (95°C for 15 s, and 60°C for 1 min) were used. RNA quantity was calculated from the cycle number by using primer-specific standard curves. Primer sets designed to span exon junctions were as follows: DOCK8 forward (F), 5′-TCAGCCTCTGTGGGTAGACA-3′, and reverse (R), 5′-CCGCACAAAGAGATTTTGGA-3′; CDC42 F, 5′-CGCCCA-CAACAACACACTTA-3′, and R, 5′-CCCGGTGGAGAAGCTGAG-3′; RAC1 F, 5′-TCTCCAGGAAATGCATTGGT-3′, and R, 5′-CTGATG-CAGGCCATCAAGT-3′; RAC2 F, 5′-TTGCTGTCCACCATCA-CATT-3′, and R, 5′-AGACCTGCCTTCTCATCAGC-3′; and β-actin F, 5′-GTTGTCGACGACGAGCG-3′, and R, 5′-GCACAGAGCCTC-GCCTT-3′. Expression of each gene was normalized to the β-actin housekeeping gene. Knockdown efficiencies of genes were calculated as normalized levels in T cells transfected with indicated siRNA, divided by normalized levels in T cells transfected with nonspecific siRNA.

Collagen gel migration assays for morphological analyses. Collagen solution from bovine skin (Sigma-Aldrich) was mixed with 10× RPMI 1640 medium (Life Technologies) and FBS, to a final concentration of 3.6 mg/ml (unless otherwise indicated) of collagen, 1× RPMI, and 10% FBS. L-glutamine, penicillin, streptomycin, and 200 U/ml of recombinant human IL-2 were also added. The collagen mixture was stored at 4°C for no more than 10 d before use. Cells were then admixed at a final concentration of up to ∼5 × 10^7 cells/ml and the collagen gel matrix polymerized at 37°C for at least 1 h in Lab-Tek II 8-well chambered coverglasses (Nunc). In initial experiments, addition to bovine skin collagen of fibronectin at 6 μg/ml and mouse laminin at 2.5 μg/ml (both from Life Technologies), or substitution of Cultrex rat tail collagen (Trevigen) for bovine skin collagen, made no difference. Therefore, bovine collagen alone was used in all subsequent experiments.

Where indicated, small molecule inhibitors, or DMSO used as a vehicle control, were mixed with the collagen matrix at 4°C, before addition of cells and polymerization of gels. Minimal doses that exerted effects while avoiding nonspecific toxicity were used. In some experiments, Z-Val-Ala-Asp (OMe)-FMK (zVAD) (MP Biomedicals) was added at 40 or 80 μM to gels for 12–18 h to inhibit caspase activation. The class I PAK inhibitor IPA3 (Sigma-Aldrich) was used to pretreat cells at 5 μm for 30 min but was not added to gels to minimize cell toxicity. In other experiments, anti–β1-integrin (ITGB1 or CD29) antibodies (clone P5D2), which have been shown to block adhesion to collagen (Blaschke et al., 2002; Mukhopadhyay et al., 2004), were added to the gels at a final concentration of 20 μg/ml (R&D Systems).

After polymerization of gels, cells were allowed to migrate within the gels at 37°C in the presence of humidified 5% CO_2. Migrating cells were visualized by diffusion interference contrast (DIC) microscopy using an AF6000 LX microscope (Leica) on a motorized stage, with either a 20× dry objective lens or a 63× glycerol immersion objective lens. Images were acquired at 30-s intervals. Post-capture analysis was conducted with Imaris 7.0 software (Bitplane). Length was determined by measuring the distance between cell front and uropod. Width was determined by measuring the middle point across the cell body. Cells were defined as abnormally elongated if cell length was ≥8× the cell width at its midpoint. Abnormal elongation was reported either as percentage of time elongated or percentage of cells elongated. To calculate percentage of time elongated, at least 30 min of captured live images were analyzed. For each sample, cells were numbered and 20–30 cells were randomly chosen using an online random number generator. The lengths and widths of these cells were measured in each frame. The percentage of time each individual cell spent abnormally elongated was calculated, which in turn was used to calculate the mean value for the sampled cells from each patient. To calculate percentage of cells elongated, at least 3 h of captured live images were analyzed. Four time points that divided up the total time imaged into equal time intervals, and three z-steps associated with each time point, were selected for analysis. The lengths and widths of all the cells in the view at these four time points were measured. The average proportion of cells that were abnormally elongated was calculated from the sampled time points from each patient. Approximately 150–300 cells were analyzed by this latter method. The percentage of cells with elongated nucleus was calculated similar to the percent of cells elongated, except that Hoechst dye 33342 was used to stain nuclei and nuclei were classified as elongated as determined by binary scoring of blinded samples.

Immunofluorescence. T cells migrating within the collagen gel matrix were fixed with prewarmed 4% paraformaldehyde (Electron Microscopy Sciences) in PBS. The collagen gel containing the cells was washed in PBS, permeabilized with 0.5% Triton X-100, blocked with 2% bovine serum albumin (Sigma-Aldrich) in 0.1% Triton X-100, and incubated with primary antibodies for 1 h at 4°C. Anti–α-Tubulin–Alexa Fluor 488 (Life Technologies) was used with anti-pericentrin antibody (Abcam), followed by Alexa Fluor 647–conjugated anti–rabbit secondary antibody (Life Technologies). Hoechst dye 33342 at 1 μg/ml (Life Technologies) was also used. Stained gels were kept in PBS at 4°C for no longer than 24 h before image capture. Imaging was performed on a Leica SP8 or SP5 white light laser confocal microscope with a 63× glycerol immersion objective lens, using an image stack vertical step

setting of 0.15–0.2 μm. Where indicated, after staining gels were physically compressed to facilitate simultaneous visualization of all vertical stacks.

Cell cycle analysis. Cell cycle analysis was performed according to standard protocols (Darzynkiewicz and Huang, 2004). In brief, after fixation in 70% ethanol on ice for 2 h, cells were stained with 20 μg/ml of PI in PBS containing 0.1% Triton-100 and 0.2 mg/ml DNase-free RNase A (QIAGEN) at 37°C for 15 min. DNA content was acquired on a FACSCanto using a linear fluorescence amplification scale. Area versus width was used to gate out doublets. To calculate cell cycle, data were analyzed by using the Dean-Jett-Fox model on the Cell Cycle analysis platform of FlowJo.

Cell cycle blockade. Patient cells that had been expanded in culture were enriched for viable cells by Ficoll-Paque PLUS density gradient centrifugation before use in experiments. Cells were treated for 48 h with aphidicolin at 2 μg/ml (Sigma-Aldrich) or were treated with DMSO. Cells were kept in the presence or absence of aphidicolin when mixed into the collagen mixture and the gel allowed to polymerize. After migration for 2–4 h in the gel, cells were visualized by DIC microscopy to calculate the percent of cells elongated, as described above. Alternatively, cells were fixed in the gel using 2% paraformaldehyde and stained with Hoechst dye 33342. For abnormally elongated cells, the nuclear length was measured as a proportion of the cell's total length. From 13 to 38 elongated cells were analyzed per patient. Cell cycle analysis performed on cells recovered from the gel according to collagenase treatment showed that aphidicolin treatment decreased the percentage of cells in S/G2/M from 17.0 ± 10.5 and 13.2 ± 4.0 in pretreated controls and patients, respectively, to 1.4 ± 0.6 and 1.0 ± 0.5 in post-treated controls and patients, respectively (mean ± SD).

Chemotaxis assays. 3D chemotaxis assays were performed as described using a custom-fabricated device, with modifications (Sixt and Lämmermann, 2011). Activated T cells, resuspended in 3.6 mg/ml collagen, as described above, were loaded into the migration chamber. After polymerization of the gel matrix containing the cells, additional collagen gel, containing recombinant human CXCL12 (SDF-1α; PeproTech) at a final concentration of 400 ng/ml, was applied as a second layer within the migration chamber. Cells were visualized over 30 min as they migrated toward the chemokine gradient at 37°C in the presence of humidified CO_2. Time-lapse DIC images of migrating cells were acquired using a microscope (AF6000 LX; Leica) at intervals of 30 s. Cell images were loaded into Imaris 7.0, and individual cells were tracked using the "Track Spots" feature in the DIC channel. The estimated diameter of the cells was 8 μm, and a Quality Threshold for the spots was typically around 100. Tracks of the individual cell spots were assembled using the autoregression feature. Tracks shorter than 30 time points, or in which the cell displaced less than 5 μm, were excluded. The path traveled was used to calculate total displacement, displacement to the chemokine, speed, and directional velocity toward the chemokine. A total of 60–326 cells were analyzed to obtain means per sample. For statistical analysis, the values from DOCK8-deficient cells from patients and knockdowns were combined and compared with control cells and nonspecific siRNA knockdowns, using the unpaired Student's t test.

Live imaging of dying cells. In initial experiments to assess cell death, standard collagen gel matrices were set up as described above in Collagen gel migration assays for morphological analyses. DIC images were acquired at 2-min intervals for 21 h. PI was added during the last 4.5 h and allowed to diffuse into the gel, during which time simultaneous DIC and fluorescence images were acquired at 5–10 min intervals.

In subsequent experiments, mini-gels were used to track the fate of cells for 16 h. 10 μl of collagen gel, which contained 10^4 cells, was cast into a custom-partitioned segment of a high culture-insert StemCell, ibiTreat-coated, 35 mm μ-Dish (ibidi). After polymerization, all cells within the mini-gel were visualized at 37°C in the presence of humidified 5% CO_2 by DIC microscopy. A microscope (AF6000 LX) with 20× dry objective lens and motorized stage with Tiling function was used to scan through the entire

mini-gel every 2 min. Image stacks were acquired using a Roper Coolsnap camera, using the following settings: 2 × 2 binning, 1 × 3 tiling, 8 µm vertical step, 300 µm vertical depth. After data collection, tiles were assembled using LAS EZ software (Leica) and analyzed manually using Imaris software as described above. Cells were classified as those that had died or remained alive at the end of the experiment. The amount of time each cell spent abnormally elongated was calculated from the cell length and width measurements at each time frame. Elongation episodes were also classified as those immediately preceding cell fragmentation and those that did not. The duration of each elongation episode was also measured. 20 cells, chosen randomly at the beginning of the experiment, were analyzed per sample.

Quantitation of cell death. Cells were mixed into collagen gel matrices containing varying concentrations of collagen, or in complete medium, which were both supplemented with 200 U/ml of recombinant human IL-2. At the indicated times, cells were recovered by treating samples with 1 mg/ml of collagenase (Sigma-Aldrich) with 2.5 mM $CaCl_2$ at 37°C for 1 h. To stain for cell death markers, APC-conjugated Annexin V (BD) was incubated at 4°C for 15 min with the recovered cells. PI was added right before acquisition for 30 s at high speed on the FACSCanto. The numbers of Annexin V^+, PI^+, or live (Annexin V^-, PI^-) cells were counted using FlowJo analysis software. These numbers were used to calculate the percentage of cells that were dead or dying cells, as defined by Annexin V^+ and/or PI^+.

Scanning electron microscopy. After allowing 10^5 cells to migrate within the collagen gel matrix, cells were isolated by treatment with collagenase as described above and washed with PBS. Recovered cells were resuspended in 100 µl of 0.1 M sodium cacodylate buffer and 50 µl of suspensions were settled on silicon chips (Ted Pella, Inc.) for 20 min. The silicon chips were then fixed and stored at 4°C for up to 20 h in fixative containing 2.5% glutaraldehyde and 0.1 M sodium cacodylate buffer in PBS, pH 7.4. Samples were treated for 1 h with 0.5% osmium tetroxide and 0.8% potassium ferricyanide, 1 h with 1% tannic acid, and then overnight at 4°C with 1% uranyl acetate. After a graded series of ethanol dehydration steps, the silicon chips were critical point dried (cpd 030; Bal-Tec), mounted on aluminum studs, and coated with 70 Å iridium in an IBS/e sputter coater (South Bay Technologies). Digital images were acquired at 5 kV using a SU-8000 field emission scanning electron microscope (Hitachi High Technologies).

Caspase-3 staining. For intracellular flow cytometric detection of activated caspase-3, T cells were allowed to migrate within the collagen gel matrix, or in medium, for up to 20 h. Apoptosis was induced in control cells by allowing them to migrate for 6 h within the collagen gel matrix, to which anti-FAS (clone APO-1-3) antibodies (Enzo Life Sciences) and Protein A (Sigma-Aldrich) were incorporated at 200 ng/ml. Cells were recovered from gel or medium after collagenase digestion, as described above. Cells were then fixed and permeabilized using the Cytofix/Cytoperm Fixation/Permeabilization kit (BD). Cells were incubated with a 1:10 dilution of PE-conjugated anti–active-caspase-3 antibody (BD) in Perm/Wash buffer for 30 min at 4°C. Stained cells were acquired on a FACSCanto, and percentage of positive cells was calculated using FlowJo analysis software.

Mitochondrial membrane permeability staining. Cells were loaded with 0.5 µg/ml of JC-1 (Life Technologies) at 37°C for 30 min and then washed with complete medium. Loaded cells were incorporated within a collagen gel matrix as described above, and allowed to migrate within the gel for 6 h. In some cases, apoptosis was induced in control cells by incubating JC-1–loaded cells with 200 ng/ml of anti-FAS (clone APO-1-3) antibodies and 200 ng/ml of Protein A for 20 min, before incorporating cells within the collagen gel matrix. Live cell imaging, at 37°C and in the presence of 5% CO_2, was performed using a white light laser confocal microscope (Leica), with excitation wavelength of 488 nm and an image stack vertical step setting of 0.2 µm. Loss of orange-red staining of J aggregates, with continued green staining of J monomers, was indicative of mitochondrial depolarization.

Transwell assays. Polycarbonate Transwell inserts containing 5-µm membrane pores were used in 24-well plates (Corning). Recombinant human CXCL12 (SDF-1α) at 200 ng/ml (Life Technologies) was added to the lower compartment. Control and patient T cells were loaded with 0.5 µM of Cell-Tracker Green CMFDA or CellTracker Red CMPTX (Life Technologies), and dye swaps were also performed. Cells were washed once with complete medium before placing a total of $5 × 10^4$ cells in the upper compartment. After incubating at 37°C, in humidified 5% CO_2, for 1–2 h, the insert was removed, fixed in 2% paraformaldehyde in PBS for 15 min, rinsed in PBS, and stained with Hoechst dye 33342. The membrane was carefully cut off from the insert using a sharp scalpel and mounted onto glass slides with coverslips using ProLong Gold mounting medium (Life Technologies). Cells migrating through the membrane pores were imaged using a TCS SP5 laser-scanning confocal microscope with a 63× glycerol immersion objective lens.

Agarose gel migration assays. Tissue-culture grade agarose (Sigma-Aldrich) was heated at a concentration of 2% in RPMI medium. A heating block was used to keep the mixture warm as it was diluted with prewarmed complete medium to a final concentration of 0.2% agarose. After equilibration to 37°C, cells were admixed. Gels were cast into Lab-Tek II 8–well chambered coverglasses, solidified at 4°C for 10 min, and moved back to 37°C in the presence of humidified 5% CO_2. After migration within the agarose gel matrix, live cell imaging and analysis was performed as described above in Collagen gel migration assays.

2D migration assays. Lab-Tek II 8–well chambered coverglasses (Nunc) were coated with 3 µg/ml of recombinant human ICAM-2/Fc chimera (R&D Systems) overnight at 4°C and rinsed with PBS before use. Alternatively, collagen-coated slides were stored at 4°C until use (BD). 200 µl of cycling T cells (10^5/ml) were gently added into each well. After 1 h incubation at 37°C in the presence of humidified 5% CO_2, time-lapse DIC microscopy and analysis was performed as described above in Collagen gel migration assays for morphological analyses.

HSV-1 stocks and titers. To generate cell-free virus stocks of the KOS laboratory-adapted strain of HSV-1 (gift from J. Cohen, NIAID, NIH, Bethesda, MD), $1.2 × 10^7$ Vero cells grown in DMEM medium were seeded 1 d earlier to obtain a confluent monolayer. $2 × 10^4$ pfu of virus was used to infect the Vero cells. Virus was allowed to replicate while cells were cultured for 2 d at 37°C, in the presence of humidified 5% CO_2. To harvest the virus, the infected cells were collected into the medium using a cell scraper, and centrifuged briefly at 4°C. The pellet was frozen on dry ice and thawed for three cycles. After centrifugation at 4°C, the supernatant was aliquoted and stored at −80°C until use.

Virus stocks were quantitated using a standard plaque assay. Vero cells were seeded at $5 × 10^5$ cells per well in 6-well plates, 1 d earlier. An aliquot of virus stock was thawed on ice and a 10-fold dilution series was made in medium. In each well, 500 µl of the diluted virus was added to a total volume of 1 ml, and virus allowed to adsorb for 1 h. Cells were overlaid with medium containing human gamma globulin (Gamunex-C, Talecris) and cultured for 2 d. The medium was removed, and cells were stained for 1 h at room temperature with 1% crystal violet in 10% formaldehyde, 5% acetic acid, and 60% methanol. After washing with water and air-drying, the plaques in the cell monolayers were counted. The PFU/ml of the virus stock was calculated as: (number of plaques in one well) × 2 × (fold of dilution of virus stock used for infection).

HSV-1 infections. Mice were infected epicutaneously as previously described (Goel et al., 2002; van Lint et al., 2004; Gebhardt et al., 2011). Sex-matched mice, at 6–8 wk of age, were used for infections, with four to seven mice per treatment group in each experiment. In brief, mice were anesthetized with an intraperitoneal injection of 2.5 mg ketamine and 0.4 mg xylazine in sterile PBS, per 20 g of body weight. The fur was clipped and depilated with Nair in the region of the dorsal left flank. The skin was then abraded

using a 1.5 × 1.5 mm square, 100 grit sand paper (3M), with 10 steady strokes of manually applied pressure. HSV-1, at 10^6 pfu in a volume of 5 µl, was dropped onto the abraded skin, and the site of infection covered for 12 h. Disease severity was scored daily according to the following criteria: 0, no symptoms; 1, several isolated blisters close to the original infection site; 2, blisters clustered along a dermatomal distribution to form a continuous line; 3, blisters merged together with extensive necrosis surrounding the blisters; 4, mouse found dead or with neurological symptoms requiring euthanasia.

Adoptive transfers of T cells. CD8 T cells were isolated and enriched from DOCK8-deficient GFP-cpm mice by incubating splenocytes with an antibody cocktail (Ter119, M5/114, GK1.5, RB6-8C5, M1/70, and F4/80) and performing negative enrichment with Dynabead magnetic beads (Invitrogen). These T cells were adoptively transferred into C57BL/6 mice (3 × 10^6 cells) along with 3 × 10^3 CD8 T cells from gBT-I.DsRed TCR transgenic mice, before skin HSV infection. Naive gBT-I.DsRed or gBT-I.GFP. cpm T cells isolated from LNs were adoptively transferred via the tail vein. A total of 5 × 10^4 cells were transferred in cotransfer experiments before HSV infection. In vitro–generated gBT-I and gBT-I.GFP.cpm effector splenocytes were activated by peptide-pulsed splenocytes as previously described (Mackay et al., 2012). Such cells were comparably activated by this regimen, as reflected by their CD44^{hi} and CD62L^{lo} surface marker expression, consistent with previous reports that Dock8 mutant cells activate and proliferate normally after TCR stimulation (Lambe et al., 2011). Activated CD44^{hi} T cells (10^6) were transferred into recipients by intradermal injection (five 20-µl injections over an area of skin 1 × 1.5 cm^2) with a 30-gauge needle. For DNFB (Sigma-Aldrich) treatment, mice were shaved and depilated before the application of 15 µl of 0.5% DNFB in acetone/oil (4:1) to a 1-cm^2 area of skin. 30 d after DNFB treatment, mice were infected on the skin with HSV.

Intravital two-photon microscopy. Mice were infected epicutaneously with HSV-1 and the skin imaged by two-photon microscopy as previously described (Gebhardt et al., 2011). For intravital two-photon microscopy, mice were anaesthetized, depilated, and two parallel incisions were made ∼15 mm apart along the flank. The skin was separated from the peritoneum, and adhered to an 18-mm-wide piece of 1-mm stainless steel inserted to form a stable raised platform, attached to a custom-made imaging platform maintained at 35°C. Images were acquired with an upright LSM710 NLO multiphoton microscope (Carl Zeiss) with a 20× 1.0 NA water immersion objective. 3D stacks were captured every 1 min for 30–60 min. Raw imaging data were processed with Imaris 7 (Biplane). Cell migration through combined epidermal and dermal layers was analyzed through automatic cell tracking aided by manual corrections. Only tracks that lasted longer than 5 min were analyzed. For the generation of movies, image sequences exported from Imaris were composed in After Effects (CS5; Adobe).

Statistical analyses. Figs. 2 (C–I), 4 (D and E), 5 (C and F, right), 6 (C and D), 7 (D and E), 9 E, and 10 (F and G): the unpaired two-tailed Student's t test was performed using Prism 6.0 software (GraphPad). Fig. 9 E: 17 movies from six mice pooled from two experiments were analyzed. In each movie, all the cells in the frame, numbering at least several dozen, were counted and the proportion elongated calculated. In the remaining experiments where individual cells were analyzed, the mean value for the population from each sample tested was used to represent that individual. P-values are indicated in the legends. Fig. 3 (A–D): the mean values for controls and control NS siRNA were included in the DOCK8-replete group, and the mean values for patients and knockdowns were included in the DOCK8-deficient group. For each parameter, the two groups were compared using the unpaired two-tailed Student's t test. ns, not significant (P ≥ 0.4). Figs. 4 C, 5 F (left), 6 E, 7 (B, F, and H), and 10 (A–C and E): ordinary two-way ANOVA was performed with correction for multiple comparisons using Prism. P-values are indicated in the legends. For Fig. 6 E comparisons, p-values were nonsignificant (P > 0.99). Fig. 5 C: for each individual tested, the time was plotted against percentage of active caspase-3–positive cells. The slopes of the

individual dose–response curves were calculated using the nonlinear regression curve fitting option (straight-line) in Prism. The slopes for controls migrating in gel and patients migrating in gel were 0.015 ± 0.023 and 0.13 ± 0.054, respectively, which indicated little dose-effect correlation for cells migrating in gel. In contrast, in controls induced to undergo apoptosis, the slope was 11.0 ± 1.4, which indicated a strong dose-effect correlation (mean ± SD). Fig. 6 A: a linear mixed effects model was used to compare the effect of collagen concentration on response of cells from controls versus patients. There was no dose effect in the control group, and no difference between controls and patients when dose level was 0. The dose effect at concentrations >0 was different in the controls versus the patients, as indicated by interaction of 4.736 (95% CI of 3.87, 5.61) with p-value <0.0001. Figs. 7 A and 10 H: ordinary one-way ANOVA was performed with correction for multiple comparisons, using Prism. P-values are indicated in the legends. Fig. 9 B: The Wilcoxon matched-pairs signed rank test (two-tailed) was performed using Prism to compare repeated measurements of clinical scores associated with individual Dock8-deficient (KO) versus WT mice. The p-value was 0.001. Fig. 9 C: the log-rank (Mantel-Cox) test for the Kaplan-Meier survival curve was performed using Prism. *, P = 0.016.

Online supplemental material. Videos 1 and 2 show T cell and NK cell elongation during migration within collagen gel matrices. Video 3 shows cytothripsis. Videos 4 and 5 show intravital two-photon microscopy during viral skin infections. Online supplemental material is available at http://www.jem.org/cgi/content/full/jem.20141307/DC1.

REFERENCES

Akbar, H., X. Shang, R. Perveen, M. Berryman, K. Funk, J.F. Johnson, N.N. Tandon, and Y. Zheng. 2011. Gene targeting implicates Cdc42 GTPase in GPVI and non-GPVI mediated platelet filopodia formation, secretion and aggregation. *PLoS ONE*. 6:e22117. http://dx.doi.org/10.1371/journal.pone.0022117

Ariotti, S., J.B. Beltman, G. Chodaczek, M.E. Hoekstra, A.E. van Beek, R. Gomez-Eerland, L. Ritsma, J. van Rheenen, A.F. Marée, T. Zal, et al. 2012. Tissue-resident memory CD8+ T cells continuously patrol skin epithelia to quickly recognize local antigen. *Proc. Natl. Acad. Sci. USA*. 109:19739–19744. http://dx.doi.org/10.1073/pnas.1208927109

Biron, C.A., K.B. Nguyen, G.C. Pien, L.P. Cousens, and T.P. Salazar-Mather. 1999. Natural killer cells in antiviral defense: function and regulation by innate cytokines. *Annu. Rev. Immunol*. 17:189–220. http://dx.doi.org/10.1146/annurev.immunol.17.1.189

Blaschke, F., P. Stawowy, S. Goetze, O. Hintz, M. Gräfe, U. Kintscher, E. Fleck, and K. Graf. 2002. Hypoxia activates β_1-integrin via ERK 1/2 and p38 MAP kinase in human vascular smooth muscle cells. *Biochem. Biophys. Res. Commun*. 296:890–896. http://dx.doi.org/10.1016/S0006-291X(02)02033-8

Bokoch, G.M. 2003. Biology of the p21-activated kinases. *Annu. Rev. Biochem*. 72:743–781. http://dx.doi.org/10.1146/annurev.biochem.72.121801.161742

Chu, E.Y., A.F. Freeman, H. Jing, E.W. Cowen, J. Davis, H.C. Su, S.M. Holland, and M.L. Turner. 2012. Cutaneous manifestations of *DOCK8* deficiency syndrome. *Arch. Dermatol*. 148:79–84. http://dx.doi.org/10.1001/archdermatol.2011.262

Côté, J.F., and K. Vuori. 2002. Identification of an evolutionarily conserved superfamily of DOCK180-related proteins with guanine nucleotide exchange activity. *J. Cell Sci*. 115:4901–4913. http://dx.doi.org/10.1242/jcs.00219

Côté, J.F., and K. Vuori. 2007. GEF what? Dock180 and related proteins help Rac to polarize cells in new ways. *Trends Cell Biol*. 17:383–393. http://dx.doi.org/10.1016/j.tcb.2007.05.001

Crawford, G., A. Enders, U. Gileadi, S. Stankovic, Q. Zhang, T. Lambe, T.L. Crockford, H.E. Lockstone, A. Freeman, P.D. Arkwright, et al. 2013. DOCK8 is critical for the survival and function of NKT cells. *Blood*. 122:2052–2061. http://dx.doi.org/10.1182/blood-2013-02-482331

Cunningham, A.L., R.R. Turner, A.C. Miller, M.F. Para, and T.C. Merigan. 1985. Evolution of recurrent herpes simplex lesions. An immunohistologic study. *J. Clin. Invest*. 75:226–233. http://dx.doi.org/10.1172/JCI111678

Darzynkiewicz, Z., and X. Huang. 2004. Analysis of cellular DNA content by flow cytometry. *Curr. Protoc. Immunol*. Chapter 5:7.

De Meester, J., R. Calvez, S. Valitutti, and L. Dupré. 2010. The Wiskott-Aldrich syndrome protein regulates CTL cytotoxicity and is required for efficient killing of B cell lymphoma targets. *J. Leukoc. Biol*. 88:1031–1040. http://dx.doi.org/10.1189/jlb.0410197

Dotta, L., L. Tassone, and R. Badolato. 2011. Clinical and genetic features of Warts, Hypogammaglobulinemia, Infections and Myelokathexis (WHIM) syndrome. *Curr. Mol. Med*. 11:317–325. http://dx.doi.org/10.2174/156652411795677963

Drijkoningen, M., C. De Wolf-Peeters, H. Degreef, and V. Desmet. 1988. Epidermal Langerhans cells, dermal dendritic cells, and keratinocytes in viral lesions of skin and mucous membranes: an immunohistochemical study. *Arch. Dermatol. Res*. 280:220–227. http://dx.doi.org/10.1007/BF00513961

Dustin, M.L. 2008. Hunter to gatherer and back: immunological synapses and kinapses as variations on the theme of amoeboid locomotion. *Annu. Rev. Cell Dev. Biol*. 24:577–596. http://dx.doi.org/10.1146/annurev.cellbio.24.110707.175226

Ebert, L.M., S. Meuter, and B. Moser. 2006. Homing and function of human skin γδ T cells and NK cells: relevance for tumor surveillance. *J. Immunol*. 176:4331–4336. http://dx.doi.org/10.4049/jimmunol.176.7.4331

Engelhardt, K.R., S. McGhee, S. Winkler, A. Sassi, C. Woellner, G. Lopez-Herrera, A. Chen, H.S. Kim, M.G. Lloret, I. Schulze, et al. 2009. Large deletions and point mutations involving the dedicator of cytokinesis 8 (DOCK8) in the autosomal-recessive form of hyper-IgE

syndrome. *J. Allergy Clin. Immunol*. 124:1289–1302: e4. http://dx.doi.org/10.1016/j.jaci.2009.10.038

Friedl, P., K. Wolf, and J. Lammerding. 2011. Nuclear mechanics during cell migration. *Curr. Opin. Cell Biol*. 23:55–64. http://dx.doi.org/10.1016/j.ceb.2010.10.015

Gebhardt, T., L.M. Wakim, L. Eidsmo, P.C. Reading, W.R. Heath, and F.R. Carbone. 2009. Memory T cells in nonlymphoid tissue that provide enhanced local immunity during infection with herpes simplex virus. *Nat. Immunol*. 10:524–530. http://dx.doi.org/10.1038/ni.1718

Gebhardt, T., P.G. Whitney, A. Zaid, L.K. Mackay, A.G. Brooks, W.R. Heath, F.R. Carbone, and S.N. Mueller. 2011. Different patterns of peripheral migration by memory CD4+ and CD8+ T cells. *Nature*. 477: 216–219. http://dx.doi.org/10.1038/nature10339

Goel, N., J.J. Docherty, M.M. Fu, D.H. Zimmerman, and K.S. Rosenthal. 2002. A modification of the epidermal scarification model of herpes simplex virus infection to achieve a reproducible and uniform progression of disease. *J. Virol. Methods*. 106:153–158. http://dx.doi.org/10.1016/S0166-0934(02)00160-X

Gotoh, K., Y. Tanaka, A. Nishikimi, A. Inayoshi, M. Enjoji, R. Takayanagi, T. Sasazuki, and Y. Fukui. 2008. Differential requirement for DOCK2 in migration of plasmacytoid dendritic cells versus myeloid dendritic cells. *Blood*. 111:2973–2976. http://dx.doi.org/10.1182/blood-2007-09-112169

Grégoire, C., L. Chasson, C. Luci, E. Tomasello, F. Geissmann, E. Vivier, and T. Walzer. 2007. The trafficking of natural killer cells. *Immunol. Rev*. 220:169–182. http://dx.doi.org/10.1111/j.1600-065X.2007.00563.x

Guo, F., D. Hildeman, P. Tripathi, C.S. Velu, H.L. Grimes, and Y. Zheng. 2010. Coordination of IL-7 receptor and T-cell receptor signaling by cell-division cycle 42 in T-cell homeostasis. *Proc. Natl. Acad. Sci. USA*. 107:18505–18510. http://dx.doi.org/10.1073/pnas.1010249107

Ham, H., S. Guerrier, J. Kim, R.A. Schoon, E.L. Anderson, M.J. Hamann, Z. Lou, and D.D. Billadeau. 2013. Dedicator of cytokinesis 8 interacts with talin and Wiskott-Aldrich syndrome protein to regulate NK cell cytotoxicity. *J. Immunol*. 190:3661–3669. http://dx.doi.org/10.4049/jimmunol.1202792

Harada, Y., Y. Tanaka, M. Terasawa, M. Pieczyk, K. Habiro, T. Katakai, K. Hanawa-Suetsugu, M. Kukimoto-Niino, T. Nishizaki, M. Shirouzu, et al. 2012. DOCK8 is a Cdc42 activator critical for interstitial dendritic cell migration during immune responses. *Blood*. 119:4451–4461. http://dx.doi.org/10.1182/blood-2012-01-407098

Harpaz, R., I.R. Ortega-Sanchez, and J.F. Seward. Advisory Committee on Immunization Practices (ACIP) Centers for Disease Control and Prevention (CDC). 2008. Prevention of herpes zoster: recommendations of the Advisory Committee on Immunization Practices (ACIP). *MMWR Recomm. Rep*. 57:1–30, quiz :CE2–CE4.

Higgins, C.R., J.K. Schofield, F.M. Tatnall, and I.M. Leigh. 1993. Natural history, management and complications of herpes labialis. *J. Med. Virol*. 41:22–26. http://dx.doi.org/10.1002/jmv.1890410506

Honda, T., J.G. Egen, T. Lämmermann, W. Kastenmüller, P. Torabi-Parizi, and R.N. Germain. 2014. Tuning of antigen sensitivity by T cell receptor-dependent negative feedback controls T cell effector function in inflamed tissues. *Immunity*. 40:235–247. http://dx.doi.org/10.1016/j.immuni.2013.11.017

Imai, K., T. Morio, Y. Zhu, Y. Jin, S. Itoh, M. Kajiwara, J. Yata, S. Mizutani, H.D. Ochs, and S. Nonoyama. 2004. Clinical course of patients with WASP gene mutations. *Blood*. 103:456–464. http://dx.doi.org/10.1182/blood-2003-05-1480

Jabara, H.H., D.R. McDonald, E. Janssen, M.J. Massaad, N. Ramesh, A. Borzutzky, I. Rauter, H. Benson, L. Schneider, S. Baxi, et al. 2012. DOCK8 functions as an adaptor that links TLR–MyD88 signaling to B cell activation. *Nat. Immunol*. 13:612–620. http://dx.doi.org/10.1038/ni.2305

Jaffe, A.B., and A. Hall. 2005. Rho GTPases: biochemistry and biology. *Annu. Rev. Cell Dev. Biol*. 21:247–269. http://dx.doi.org/10.1146/annurev.cellbio.21.020604.150721

Jiang, X., R.A. Clark, L. Liu, A.J. Wagers, R.C. Fuhlbrigge, and T.S. Kupper. 2012. Skin infection generates non–migratory memory CD8+ T(RM) cells providing global skin immunity. *Nature*. 483:227–231. http://dx.doi.org/10.1038/nature10851

2564

DOCK8 and cytothripsis in skin viral infections | Zhang et al.

Jing, H., Q. Zhang, Y. Zhang, B.J. Hill, C.G. Dove, E.W. Gelfand, T.P. Atkinson, G. Uzel, H.F. Matthews, P.J. Mustillo, et al. 2014. Somatic reversion in dedicator of cytokinesis 8 immunodeficiency modulates disease phenotype. *J. Allergy Clin. Immunol.* 133:1667–1675. http://dx.doi.org/10.1016/j.jaci.2014.03.025

Kikuchi, T., S. Kubonishi, M. Shibakura, N. Namba, T. Matsui, Y. Fukui, M. Tanimoto, and Y. Katayama. 2008. Dock2 participates in bone marrow lympho-hematopoiesis. *Biochem. Biophys. Res. Commun.* 367:90–96. http://dx.doi.org/10.1016/j.bbrc.2007.12.093

Kilkenny, M., and R. Marks. 1996. The descriptive epidemiology of warts in the community. *Australas. J. Dermatol.* 37:80–86. http://dx.doi.org/10.1111/j.1440-0960.1996.tb01010.x

Kittler, R., L. Pelletier, A.K. Heninger, M. Slabicki, M. Theis, L. Miroslaw, I. Poser, S. Lawo, H. Grabner, K. Kozak, et al. 2007. Genome-scale RNAi profiling of cell division in human tissue culture cells. *Nat. Cell Biol.* 9:1401–1412. http://dx.doi.org/10.1038/ncb1659

Kunisaki, Y., A. Nishikimi, Y. Tanaka, R. Takii, M. Noda, A. Inayoshi, K. Watanabe, F. Sanematsu, T. Sasazuki, T. Sasaki, and Y. Fukui. 2006. DOCK2 is a Rac activator that regulates motility and polarity during neutrophil chemotaxis. *J. Cell Biol.* 174:647–652. http://dx.doi.org/10.1083/jcb.200602142

Lambe, T., G. Crawford, A.L. Johnson, T.L. Crockford, T. Bouriez-Jones, A.M. Smyth, T.H. Pham, Q. Zhang, A.F. Freeman, J.G. Cyster, et al. 2011. DOCK8 is essential for T-cell survival and the maintenance of CD8+ T-cell memory. *Eur. J. Immunol.* 41:3423–3435. http://dx.doi.org/10.1002/eji.201141759

Lämmermann, T., B.L. Bader, S.J. Monkley, T. Worbs, R. Wedlich-Söldner, K. Hirsch, M. Keller, R. Förster, D.R. Critchley, R. Fässler, and M. Sixt. 2008. Rapid leukocyte migration by integrin-independent flowing and squeezing. *Nature.* 453:51–55. http://dx.doi.org/10.1038/nature06887

Lang, P.A., N. Shaabani, S. Borkens, N. Honke, S. Scheu, S. Booth, D. Brenner, A. Meryk, C. Barthuber, M. Recher, et al. 2013. Reduced type I interferon production by dendritic cells and weakened antiviral immunity in patients with Wiskott-Aldrich syndrome protein deficiency. *J. Allergy Clin. Immunol.* 131:815–824: 824.e2. http://dx.doi.org/10.1016/j.jaci.2012.08.050

Li, R., and G.G. Gundersen. 2008. Beyond polymer polarity: how the cytoskeleton builds a polarized cell. *Nat. Rev. Mol. Cell Biol.* 9:860–873. http://dx.doi.org/10.1038/nrm2522

Lowry, O.H., D.R. Gilligan, and E.M. Katersky. 1941. The determination of collagen and elastin in tissues, with results obtained in various normal tissues from different species. *J. Biol. Chem.* 139:795–804.

Mackay, L.K., A.T. Stock, J.Z. Ma, C.M. Jones, S.J. Kent, S.N. Mueller, W.R. Heath, F.R. Carbone, and T. Gebhardt. 2012. Long-lived epithelial immunity by tissue-resident memory T (TRM) cells in the absence of persisting local antigen presentation. *Proc. Natl. Acad. Sci. USA.* 109:7037–7042. http://dx.doi.org/10.1073/pnas.1202288109

Mackay, L.K., A. Rahimpour, J.Z. Ma, N. Collins, A.T. Stock, M.L. Hafon, J. Vega-Ramos, P. Lauzurica, S.N. Mueller, T. Stefanovic, et al. 2013. The developmental pathway for CD103+CD8+ tissue-resident memory T cells of skin. *Nat. Immunol.* 14:1294–1301. http://dx.doi.org/10.1038/ni.2744

Meller, N., S. Merlot, and C. Guda. 2005. CZH proteins: a new family of Rho-GEFs. *J. Cell Sci.* 118:4937–4946. http://dx.doi.org/10.1242/jcs.02671

Mizesko, M.C., P.P. Banerjee, L. Monaco-Shawver, E.M. Mace, W.E. Bernal, J. Sawalle-Belohradsky, B.H. Belohradsky, V. Heinz, A.F. Freeman, K.E. Sullivan, et al. 2013. Defective actin accumulation impairs human natural killer cell function in patients with dedicator of cytokinesis 8 deficiency. *J. Allergy Clin. Immunol.* 131:840–848. http://dx.doi.org/10.1016/j.jaci.2012.12.1568

Mou, F., M. Praskova, F. Xia, D. Van Buren, H. Hock, J. Avruch, and D. Zhou. 2012. The Mst1 and Mst2 kinases control activation of rho family GTPases and thymic egress of mature thymocytes. *J. Exp. Med.* 209:741–759. http://dx.doi.org/10.1084/jem.20111692

Mueller, S.N., W. Heath, J.D. McLain, F.R. Carbone, and C.M. Jones. 2002. Characterization of two TCR transgenic mouse lines specific for herpes simplex virus. *Immunol. Cell Biol.* 80:156–163. http://dx.doi.org/10.1046/j.1440-1711.2002.01071.x

Mueller, S.N., T. Gebhardt, F.R. Carbone, and W.R. Heath. 2013. Memory T cell subsets, migration patterns, and tissue residence. *Annu. Rev. Immunol.* 31:137–161. http://dx.doi.org/10.1146/annurev-immunol-032712-095954

Mukhopadhyay, N.K., D. Gilchrist, G.J. Gordon, C.J. Chen, R. Bueno, M.L. Lu, R. Salgia, D.J. Sugarbaker, and M.T. Jaklitsch. 2004. Integrin-dependent protein tyrosine phosphorylation is a key regulatory event in collagen-IV-mediated adhesion and proliferation of human lung tumor cell line, Calu-1. *Ann. Thorac. Surg.* 78:450–457. http://dx.doi.org/10.1016/j.athoracsur.2004.01.042

Muraki, R., T. Baba, T. Iwasaki, T. Sata, and T. Kurata. 1992. Immunohistochemical study of skin lesions in herpes zoster. *Virchows Arch. A Pathol. Anat. Histopathol.* 420:71–76. http://dx.doi.org/10.1007/BF01605987

Neuman, R.E., and M.A. Logan. 1950. The determination of collagen and elastin in tissues. *J. Biol. Chem.* 186:549–556.

Nikkels, A.F., P. Delvenne, C. Sadzot-Delvaux, S. Debrus, J. Piette, B. Rentier, G. Lipcsei, P. Quatresooz, and G.E. Piérard. 1996. Distribution of varicella zoster virus and herpes simplex virus in disseminated fatal infections. *J. Clin. Pathol.* 49:243–248. http://dx.doi.org/10.1136/jcp.49.3.243

Nishikimi, A., H. Fukuhara, W. Su, T. Hongu, S. Takasuga, H. Mihara, Q. Cao, F. Sanematsu, M. Kanai, H. Hasegawa, et al. 2009. Sequential regulation of DOCK2 dynamics by two phospholipids during neutrophil chemotaxis. *Science.* 324:384–387. http://dx.doi.org/10.1126/science.1170179

Nishikimi, A., M. Kukimoto-Niino, S. Yokoyama, and Y. Fukui. 2013. Immune regulatory functions of DOCK family proteins in health and disease. *Exp. Cell Res.* 319:2343–2349. http://dx.doi.org/10.1016/j.yexcr.2013.07.024

Pedersen, J.A., and M.A. Swartz. 2005. Mechanobiology in the third dimension. *Ann. Biomed. Eng.* 33:1469–1490. http://dx.doi.org/10.1007/s10439-005-8159-4

Randall, K.L., T. Lambe, A.L. Johnson, B. Treanor, E. Kucharska, H. Domaschenz, B. Whittle, L.E. Tze, A. Enders, T.L. Crockford, et al. 2009. Dock8 mutations cripple B cell immunological synapses, germinal centers and long-lived antibody production. *Nat. Immunol.* 10:1283–1291. http://dx.doi.org/10.1038/ni.1820

Randall, K.L., S.S. Chan, C.S. Ma, I. Fung, Y. Mei, M. Yabas, A. Tan, P.D. Arkwright, W. Al Suwairi, S.O. Lugo Reyes, et al. 2011. DOCK8 deficiency impairs CD8 T cell survival and function in humans and mice. *J. Exp. Med.* 208:2305–2320. http://dx.doi.org/10.1084/jem.20110345

Ruusala, A., and P. Aspenström. 2004. Isolation and characterisation of DOCK8, a member of the DOCK180-related regulators of cell morphology. *FEBS Lett.* 572:159–166. http://dx.doi.org/10.1016/j.febslet.2004.06.095

Sabry, A., P.J. Hauk, H. Jing, H.C. Su, N.V. Stence, D.M. Mirsky, M.A. Nagel, J.K. Abbott, L.L. Dragone, J. Armstrong-Wells, et al. 2014. Vaccine strain varicella-zoster virus-induced central nervous system vasculopathy as the presenting feature of DOCK8 deficiency. *J. Allergy Clin. Immunol.* 133:1225–1227. http://dx.doi.org/10.1016/j.jaci.2013.11.031

Sanal, O., H. Jing, T. Ozgur, D. Ayvaz, D.M. Strauss-Albee, S. Ersoy-Evans, I. Tezcan, G. Turkkani, H.F. Matthews, G. Haliloglu, et al. 2012. Additional diverse findings expand the clinical presentation of DOCK8 deficiency. *J. Clin. Immunol.* 32:698–708. http://dx.doi.org/10.1007/s10875-012-9664-5

Schaefer, B.C., M.L. Schaefer, J.W. Kappler, P. Marrack, and R.M. Kedl. 2001. Observation of antigen-dependent CD8+ T-cell/dendritic cell interactions in vivo. *Cell. Immunol.* 214:110–122. http://dx.doi.org/10.1006/cimm.2001.1895

Simmons, A., and A.A. Nash. 1984. Zosteriform spread of herpes simplex virus as a model of recrudescence and its use to investigate the role of immune cells in prevention of recurrent disease. *J. Virol.* 52:816–821.

Sinha, S., and W. Yang. 2008. Cellular signaling for activation of Rho GTPase Cdc42. *Cell. Signal.* 20:1927–1934. http://dx.doi.org/10.1016/j.cellsig.2008.05.002

Sixt, M., and T. Lämmermann. 2011. In vitro analysis of chemotactic leukocyte migration in 3D environments. *Methods Mol. Biol.* 769:149–165. http://dx.doi.org/10.1007/978-1-61779-207-6_11

JEM

Snapper, S.B., P. Meelu, D. Nguyen, B.M. Stockton, P. Bozza, F.W. Alt, F.S. Rosen, U.H. von Andrian, and C. Klein. 2005. WASP deficiency leads to global defects of directed leukocyte migration in vitro and in vivo. *J. Leukoc. Biol.* 77:993–998. http://dx.doi.org/10.1189/jlb.0804444

Spinner, M.A., L.A. Sanchez, A.P. Hsu, P.A. Shaw, C.S. Zerbe, K.R. Calvo, D.C. Arthur, W. Gu, C.M. Gould, C.C. Brewer, et al. 2014. GATA2 deficiency: a protean disorder of hematopoiesis, lymphatics, and immunity. *Blood.* 123:809–821. http://dx.doi.org/10.1182/blood-2013-07-515528

Stock, A.T., J.M. Smith, and F.R. Carbone. 2014. Type I IFN suppresses Cxcr2 driven neutrophil recruitment into the sensory ganglia during viral infection. *J. Exp. Med.* 211:751–759. http://dx.doi.org/10.1084/jem.20132183

Su, H.C., H. Jing, and Q. Zhang. 2011. DOCK8 deficiency. *Ann. N.Y. Acad. Sci.* 1246:26–33. http://dx.doi.org/10.1111/j.1749-6632.2011.06295.x

Sullivan, K.E., C.A. Mullen, R.M. Blaese, and J.A. Winkelstein. 1994. A multiinstitutional survey of the Wiskott-Aldrich syndrome. *J. Pediatr.* 125:876–885. http://dx.doi.org/10.1016/S0022-3476(05)82002-5

van Lint, A., M. Ayers, A.G. Brooks, R.M. Coles, W.R. Heath, and F.R. Carbone. 2004. Herpes simplex virus–specific CD8+ T cells can clear established lytic infections from skin and nerves and can partially limit the early spread of virus after cutaneous inoculation. *J. Immunol.* 172:392–397. http://dx.doi.org/10.4049/jimmunol.172.1.392

Vintersten, K., C. Monetti, M. Gertsenstein, P. Zhang, L. Laszlo, S. Biechele, and A. Nagy. 2004. Mouse in red: red fluorescent protein expression in mouse ES cells, embryos, and adult animals. *Genesis.* 40:241–246. http://dx.doi.org/10.1002/gene.20095

Wolf, K., S. Alexander, V. Schacht, L.M. Coussens, U.H. von Andrian, J. van Rheenen, E. Deryugina, and P. Friedl. 2009. Collagen-based cell migration models in vitro and in vivo. *Semin. Cell Dev. Biol.* 20:931–941. http://dx.doi.org/10.1016/j.semcdb.2009.08.005

Zaid, A., L.K. Mackay, A. Rahimpour, A. Braun, M. Veldhoen, F.R. Carbone, J.H. Manton, W.R. Heath, and S.N. Mueller. 2014. Persistence of skin-resident memory T cells within an epidermal niche. *Proc. Natl. Acad. Sci. USA.* 111:5307–5312. http://dx.doi.org/10.1073/pnas.1322292111

Zhang, J., A. Shehabeldin, L.A. da Cruz, J. Butler, A.K. Somani, M. McGavin, I. Kozieradzki, A.O. dos Santos, A. Nagy, S. Grinstein, et al. 1999. Antigen receptor–induced activation and cytoskeletal rearrangement are impaired in Wiskott-Aldrich syndrome protein-deficient lymphocytes. *J. Exp. Med.* 190:1329–1342. http://dx.doi.org/10.1084/jem.190.9.1329

Zhang, Q., J.C. Davis, I.T. Lamborn, A.F. Freeman, H. Jing, A.J. Favreau, H.F. Matthews, J. Davis, M.L. Turner, G. Uzel, et al. 2009. Combined immunodeficiency associated with DOCK8 mutations. *N. Engl. J. Med.* 361:2046–2055. http://dx.doi.org/10.1056/NEJMoa0905506

Zhu, J., T. Peng, C. Johnston, K. Phasouk, A.S. Kask, A. Klock, L. Jin, K. Diem, D.M. Koelle, A. Wald, et al. 2013. Immune surveillance by CD8αα+ skin-resident T cells in human herpes virus infection. *Nature.* 497:494–497. http://dx.doi.org/10.1038/nature12110